Expression of Interest for
Neutrinos Scattering on Glass: NuSOnG

September 13, 2007

T. Adams[4], L. Bugel[2], J.M. Conrad[2], P.H. Fisher[6], J.A. Formaggio[6],
A. de Gouvêa[9], W.A. Loinaz[1], G. Karagiorgi[2], T.R. Kobilarcik[3], S. Kopp[13],
G. Kyle[8], D.A, Mason[3], R. Milner[6], J. G. Morfín[3], M. Nakamura[7],
D. Naples[10], P. Nienaber[11], F.I Olness[12], J.F. Owens[4], W.G. Seligman[2],
M.H. Shaevitz[2], H. Schellman[9], M.J. Syphers[3], C.Y. Tan[3],
R.G. Van de Water[5], R.K. Yamamoto[6], G.P. Zeller[5]

[1]Amherst College, Amherst, MA 01002
[2]Columbia University, New York, NY 10027
[3]Fermi National Accelerator Laboratory, Batavia IL 60510
[4]Florida State University, Tallahassee, FL 32306
[5]Los Alamos National Accelerator Laboratory, Los Alamos, NM 87545
[6]Massachusetts Institute of Technology, Cambridge, MA 02139
[7]Nagoya University, 464-01, Nagoya, Japan
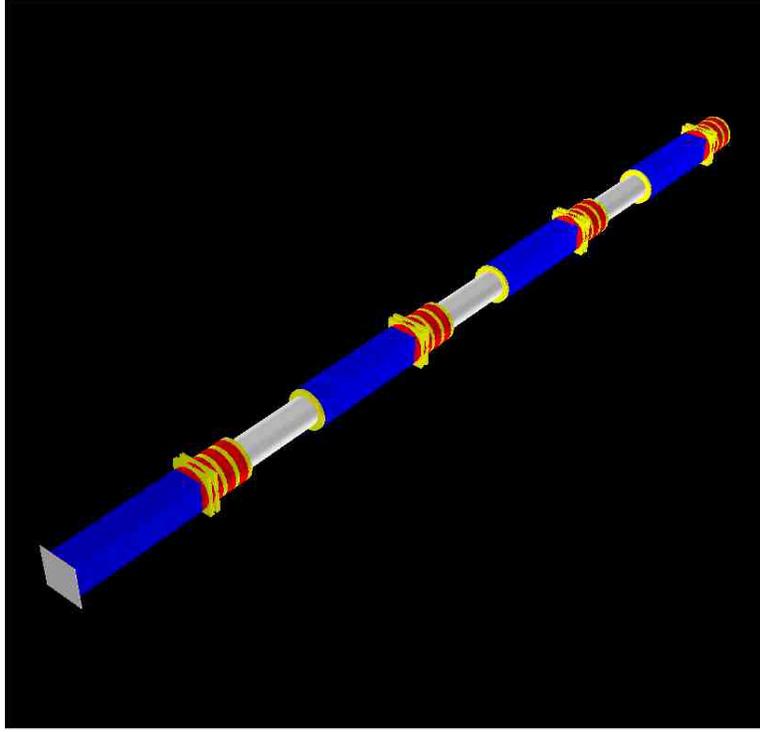[8]New Mexico State University, Las Cruces, NM 88003
[9]Northwestern University, Evanston, IL 60208
[10]University of Pittsburgh, Pittsburgh, PA 15260
[11]Saint Mary's University of Minnesota, Winona, MN 55987
[12]Southern Methodist University, Dallas, TX 75205
[13]University of Texas, Austin TX 78713

Abstract

We propose a 3500 ton (3000 ton fiducial volume) SiO_2 neutrino detector with sampling calorimetry, charged particle tracking, and muon spectrometers to run in a Tevatron Fixed Target Program. Improvements to the Fermilab accelerator complex should allow substantial increases in the neutrino flux over the previous NuTeV quad triplet beamline. With 4×10^{19} protons on target/year, a 5 year run would achieve event statistics more than 100 times higher than NuTeV. With 100 times the statistics of previous high energy neutrino experiments, the purely weak processes $\nu_\mu + e^- \rightarrow \nu_\mu + e^-$ and $\nu_\mu + e^- \rightarrow \nu_e + \mu^-$ (inverse muon decay) can be measured with high accuracy for the first time. The inverse muon decay process is independent of strong interaction effects and can be used to significantly improve the flux normalization for all other processes. The high neutrino and antineutrino fluxes also make new searches for lepton flavor violation and neutral heavy leptons possible. In this document, we give a first look at the physics opportunities, detector and beam design, and calibration procedures.

Contents

1 Introduction

The Neutrino Scattering on Glass (NuSOnG) experiment will consist of four detector modules, each composed of a finely segmented calorimeter followed by a muon spectrometer. The detector will be illuminated by a neutrino or antineutrino beam from the Tevatron. In its five-year data acquisition period, NuSOnG will make precise measurements of three types of neutrino scattering and will accumulate the world's largest sample of electron-neutrino scatters. These data will provide unique opportunities to discover physics beyond the Standard Model (including, *inter alia*, lepton flavor violation and new particles) as well as determine structure functions over a wide range of x and Q^2. The breadth of anticipated measurements makes NuSOnG a program rather than an experiment; the design heritage ensures that the approach is low-risk and cost-effective.

This Expression of Interest arises from our view that an experiment probing the high energy interactions of neutrinos is a necessary complement to the LHC and an important lead-in to the ILC. In the next few years, the LHC will reveal the nature of electroweak symmetry breaking; the Higgs mass will cease being a prediction of the electroweak theory and will become an input to the theory. Without the Higgs mass as a fit parameter, precision electroweak data, including neutrino scattering data, will be much more powerful as a tool for constraining that physics beyond the Standard Model which directly influences the electroweak sector. More important still, precision neutrino scattering will probe areas of phenomenology that may be inaccessible to the LHC and ILC. NuSOnG is not a precision test of the Standard Model; NuSOnG is a discovery experiment aimed at the terrain not covered by the collider experiments.

This Expression of Interest presents the physics case and initial design for NuSOnG. The detector draws on the heritage of FMMF, CDHS, CHARM and CCFR/NuTeV. The design uses an SiO$_2$ target in one-quarter radiation length panels interleaved with active detector elements (proportional tubes and/or scintillator). This will provide the very high segmentation needed to ensure good separation between different classes of events. We will develop these ideas in the coming months and submit a proposal to the Fermilab Directorate.

Our report is organized as follows: the physics opportunities follow in Section 2; Section 3 describes the flux and expected event rates; and Section 4 describes our preliminary design for the NuSOnG beam and apparatus. We summarize in Section 5.

2 Physics Opportunities

The physics opportunities of the experiment arise from NuSOnG's uniquely high statistics: >20k neutrino-electron scatters and >100M neutrino-quark scatters. Roughly equal statistics will be obtained from antineutrino scattering. More information on the event rates for various processes is given in Sec. 3. These rates present a wide range of physics opportunities including precision electroweak measurements, direct searches for new physics, and parton distribution studies.

2.1 Electroweak Precision Measurements

NuSOnG's considerable discovery potential derives from its ability to do precision electroweak tests through two independent channels: electron scattering and quark scattering. These measurements probe for new particles and new neutrino properties beyond the present Standard Model. As examples, NuSOnG will be sensitive to extra Z bosons with masses beyond the 1 TeV scale (depending on the model), and to compositeness scales above 5 TeV. Thus the energy scales explored by this experiment overlap the LHC, and we present the discovery potential for the new physics we will explore within this context. This experiment also directly addresses questions raised by the "NuTeV anomaly," an electroweak precision measurement in disagreement with the Standard Model.

2.1.1 Electroweak Measurements in Neutrino Scattering

NuSOnG is sensitive to new physics through neutral current (NC) scattering. The exchange of the Z boson between the neutrino ν and fermion f leads to the effective interaction:

$$
\begin{aligned}
\mathcal{L} &= -\sqrt{2}G_F \Big[\bar{\nu}\gamma_\mu(g_V^\nu - g_A^\nu\gamma_5)\nu \Big]\Big[\bar{f}\gamma^\mu(g_V^f - g_A^f\gamma_5)f \Big] \\
&= -\sqrt{2}G_F \Big[g_L^\nu\,\bar{\nu}\gamma_\mu(1-\gamma_5)\nu + g_R^\nu\,\bar{\nu}\gamma_\mu(1+\gamma_5)\nu \Big] \\
&\qquad \times \Big[g_L^f\,\bar{f}\gamma^\mu(1-\gamma_5)f + g_R^f\,\bar{f}\gamma^\mu(1+\gamma_5)f \Big] ,
\end{aligned}
\tag{1}
$$

where the Standard Model values of the couplings are:

$$
\begin{aligned}
g_L^\nu &= \sqrt{\rho}\left(+\frac{1}{2}\right) , \\
g_R^\nu &= 0 , \\
g_L^f &= \sqrt{\rho}\left(I_3^f - Q^f \sin^2\theta_W\right) , \\
g_R^f &= \sqrt{\rho}\left(-Q^f \sin^2\theta_W\right) ,
\end{aligned}
\tag{2}
$$

or equivalently,

$$
\begin{aligned}
g_V^\nu &= g_L^\nu + g_R^\nu = \sqrt{\rho}\left(+\frac{1}{2}\right) , \\
g_A^\nu &= g_L^\nu - g_R^\nu = \sqrt{\rho}\left(+\frac{1}{2}\right) ,
\end{aligned}
$$

$$
\begin{aligned}
g_V^f &= g_L^f + g_R^f = \sqrt{\rho}\left(I_3^f - 2Q^f \sin^2\theta_W\right) , \\
g_A^f &= g_L^f - g_R^f = \sqrt{\rho}\left(I_3^f\right) .
\end{aligned}
\tag{3}
$$

Here, I_3^f and Q^f are the weak isospin and electromagnetic charge of fermion f, respectively. In these formulae, ρ is the relative coupling strength of the neutral to charged current interactions ($\rho = 1$ at tree level in the Standard Model). The weak mixing parameter, $\sin^2\theta_W$, is related (at tree level) to to G_F, M_Z and α by

$$
\sin^2 2\theta_W = \frac{4\pi\alpha}{\sqrt{2}G_F M_Z^2}.
\tag{4}
$$

NuSOnG is unique in its ability to test the NC couplings by studying scattering of neutrinos from both electrons and quarks. A deviation from the Standard Model predictions in both the electron and quark measurements will present a compelling case for new physics.

Neutrino Electron Scattering

The differential cross section for muon neutrino and antineutrino scattering from electrons, defined using the coupling constants described above, is:

$$
\begin{aligned}
d\sigma = \frac{2G_F^2 m_e E_\nu}{\pi} \Big[& (g_L^\nu g_V^e \pm g_L^\nu g_A^e)^2 \frac{dT}{E_\nu} \\
& + (g_L^\nu g_V^e \mp g_L^\nu g_A^e)^2 \left(1 - \frac{T}{E_\nu}\right)^2 \frac{dT}{E_\nu} \\
& - \left\{ (g_L^\nu g_V^e)^2 - (g_L^\nu g_A^e)^2 \right\} \frac{m_e T}{E_\nu^2} \frac{dT}{E_\nu} \Big] .
\end{aligned}
\tag{5}
$$

The upper and lower signs corresponding to the neutrino and anti-neutrino cases, respectively. In this equation, E_ν is the incident ν_μ energy and T is the electron recoil kinetic energy.

More often in the literature, the cross section is defined in terms of the parameters $(g_V^{\nu e}, g_A^{\nu e})$, which are defined as

$$
\begin{aligned}
g_V^{\nu e} &\equiv (2g_L^\nu g_V^e) = \rho\left(-\frac{1}{2} + 2\sin^2\theta_W\right) , \\
g_A^{\nu e} &\equiv (2g_L^\nu g_A^e) = \rho\left(-\frac{1}{2}\right) ,
\end{aligned}
\tag{6}
$$

In terms of these parameters, we can write:

$$
\begin{aligned}
d\sigma = \frac{G_F^2 m_e E_\nu}{2\pi} \Big[& (g_V^{\nu e} \pm g_A^{\nu e})^2 \frac{dT}{E_\nu} + (g_V^{\nu e} \mp g_A^{\nu e})^2 \left(1 - \frac{T}{E_\nu}\right)^2 \frac{dT}{E_\nu} \\
& - \left\{ (g_V^{\nu e})^2 - (g_A^{\nu e})^2 \right\} \frac{m_e T}{E_\nu^2} \frac{dT}{E_\nu} \Big] ,
\end{aligned}
\tag{7}
$$

When $m_e \ll E_\nu$, the third terms in these expressions can be neglected. If we introduce the variable $y = T/E_\nu$, then

$$
\frac{d\sigma}{dy} = \frac{G_F^2 m_e E_\nu}{2\pi} \left[(g_V^{\nu e} + g_A^{\nu e})^2 + (g_V^{\nu e} - g_A^{\nu e})^2 (1 - y)^2 \right] .
\tag{8}
$$

6

Integrating over the region $0 \leq y \leq 1$, we obtain the total cross sections which are

$$\sigma = \frac{G_F^2 m_e E_\nu}{2\pi} \left[(g_V^{\nu e} \pm g_A^{\nu e})^2 + \frac{1}{3} (g_V^{\nu e} \mp g_A^{\nu e})^2 \right] . \tag{9}$$

Note that

$$\begin{aligned}
(g_V^{\nu e} + g_A^{\nu e})^2 &= \rho^2 \left(-1 + 4\sin^2 \theta_W \right)^2 = \rho^2 \left(1 - 2\sin^2 \theta_W + 4\sin^4 \theta_W \right) , \\
(g_V^{\nu e} - g_A^{\nu e})^2 &= \rho^2 \left(2\sin^2 \theta_W \right)^2 = \rho^2 \left(4\sin^4 \theta_W \right) .
\end{aligned} \tag{10}$$

Therefore,

$$\begin{aligned}
\sigma(\nu_\mu e) &= \frac{G_F^2 m_e E_\nu}{2\pi} \rho^2 \left[1 - 4\sin^2 \theta_W + \frac{16}{3} \sin^4 \theta_W \right] , \\
\sigma(\bar{\nu}_\mu e) &= \frac{G_F^2 m_e E_\nu}{2\pi} \frac{\rho^2}{3} \left[1 - 4\sin^2 \theta_W + 16\sin^4 \theta_W \right] .
\end{aligned} \tag{11}$$

The ratio of the integrated cross sections for neutrino to antineutrino electron scattering is

$$R_e = \frac{\sigma(\nu_{\mu L} e)}{\sigma(\bar{\nu}_{\mu L} e)} = 3 \frac{1 - 4\sin^2 \theta_W + \frac{16}{3} \sin^4 \theta_W}{1 - 4\sin^2 \theta_W + 16\sin^4 \theta_W} . \tag{12}$$

Many systematics, including flux errors, cancel in this ratio, as does the ρ dependence. Fig. 1(top) shows the results for $\sin^2 \theta_W$ from many past experiments.

NuSOnG will make independent measurements of the electroweak parameters for both ν_μ and $\bar{\nu}_\mu$-electron scattering. We can achieve this via ratios or by direct extraction of the cross section. In the case of ν_μ-electron scattering, we will use the ratio of the number of events in neutrino-electron elastic scattering to inverse muon decay:

$$\frac{N(\nu_\mu e^- \to \nu_\mu e^-)}{N(\nu_\mu e^- \to \mu^- \nu_e)} = \frac{\sigma_{NC}^{\nu e} \times \Phi^\nu}{\sigma^{IMD} \times \Phi^\nu}. \tag{13}$$

Because the cross section for IMD events is well determined by the standard model, this ratio should have low errors and will isolate the EW parameters from NC scattering. In the case of $\bar{\nu}_\mu$ running, the ratio is more complex because there is no equivalent process to inverse muon decay (since there are no positrons in the detector). In this case, we use the fact that, for low exchange energy in Deep Inelastic Scattering, the cross sections in neutrino and antineutrino scattering approach the same constant, A, as is explained in Sec. 3.3.2. Thus, for Deep Inelastic events with low energy transfer and hence low hadronic energy ($5 \lesssim E_{had} \lesssim 10$ GeV), $N_{\nu DIS}^{low\ E_{had}} = \Phi^\nu A$ and $N_{\bar{\nu} DIS}^{low\ E_{had}} = \Phi^{\bar{\nu}} A$. The result is that we can extract the electroweak parameters to high precision using the ratio:

$$\frac{N_{\nu DIS}^{low\ E_{had}}}{N_{\bar{\nu} DIS}^{low\ E_{had}}} \times \frac{N(\bar{\nu}_\mu e^- \to \bar{\nu}_\mu e^-)}{N(\nu_\mu e^- \to \mu^- \nu_e)} = \frac{\Phi^\nu}{\Phi^{\bar{\nu}}} \times \frac{\sigma_{NC}^{\bar{\nu} e} \times \Phi^{\bar{\nu}}}{\sigma^{IMD} \times \Phi^\nu}. \tag{14}$$

The first ratio cancels the DIS cross section, leaving the energy-integrated ν to $\bar{\nu}$ flux ratio. The IMD events in the denominator of the second term cancel the integrated ν flux. The NC elastic events cancel the integrated $\bar{\nu}$ flux. Alternatively, because we will have accurate knowledge of the flux as a function of the energy (see Sec. 3.3) we could directly measure the cross sections.
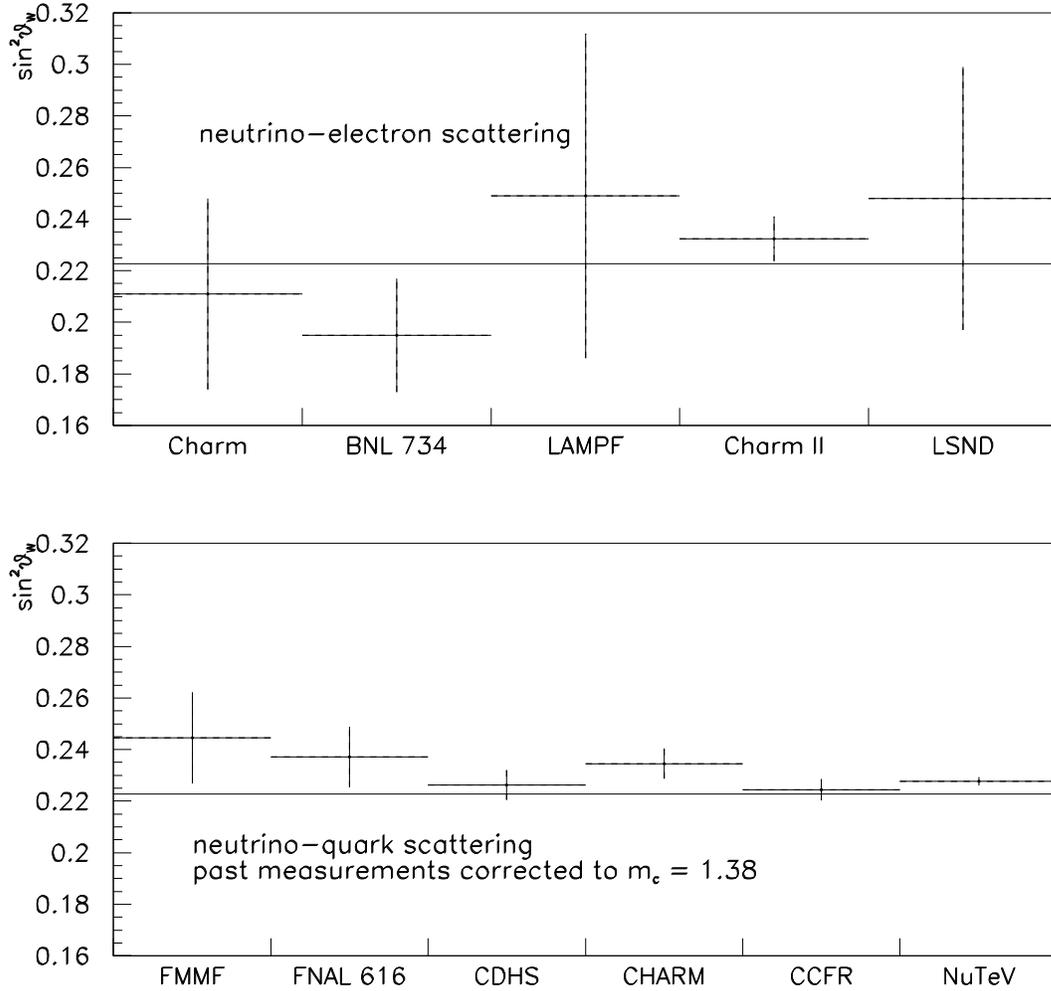
Figure 1: Measurements of $\sin^2 \theta_W$ from past experiments. Top: neutrino-electron elastic scattering experiments. Bottom: neutrino DIS experiments. All DIS results are adjusted to the same charm mass (relevant for experiments not using P-W method). The Standard Model value, indicated by the line, is 0.2227.

An important point is that the two independent measurements, one in neutrino and the other in antineutrino mode, will in turn allow independent extraction of $g_A^{\nu e}$ and $g_V^{\nu e}$. The previous best measurement from ν_μ and $\bar{\nu}_\mu$ cross-section measurements is from CHARM II, which used 2677±82 events in neutrino mode and 2752±88 events in antineutrino mode [1] to find

$$g_V^{\nu e} = -0.035 \pm 0.012(\text{stat}) \pm 0.012(\text{sys}) \tag{15}$$

$$g_A^{\nu e} = -0.503 \pm 0.006(\text{stat}) \pm 0.016(\text{sys}). \tag{16}$$

This can be compared to electroweak measurements from LEP provide a very precise prediction of these parameters [2]:

$$g_V^{\nu e} = -0.0397 \pm 0.0003 \tag{17}$$

$$g_A^{\nu e} = -0.5065 \pm 0.0001. \tag{18}$$

The CHARM II results are in agreement with LEP, but with large errors. Errors on the neutrino measurement must be substantially reduced in order to meaningfully probe for physics beyond the Standard Model. The goal of NuSOnG is to measure the neutrino-electron and antineutrino-electron cross sections to 0.7%.

2.1.1.1   *Neutrino Quark Scattering*

Substantially higher precision has been obtained using neutrino-quark scattering, which compares neutral-current (NC) to charged-current (CC) scattering to extract $\sin^2 \theta_W$. However, these experiments are subject to issues of modeling in the quark sector. Fig. 1(bottom) reviews the history of these measurements.

The lowest systematic errors come from implementing a "Paschos-Wolfenstein style" [3] analysis, which would be the technique used by NuSOnG. This requires separated ν and $\bar{\nu}$ beams, for which the following ratios could be formed:

$$R^\nu = \frac{\sigma_{NC}^\nu}{\sigma_{CC}^\nu} \tag{19}$$

$$R^{\bar{\nu}} = \frac{\sigma_{NC}^{\bar{\nu}}}{\sigma_{CC}^{\bar{\nu}}}. \tag{20}$$

$$\tag{21}$$

Paschos and Wolfenstein [3] recast these as:

$$R^- = \frac{\sigma_{NC}^\nu - \sigma_{NC}^{\bar{\nu}}}{\sigma_{CC}^\nu - \sigma_{CC}^{\bar{\nu}}} = \frac{R^\nu - r R^{\bar{\nu}}}{1 - r}, \tag{22}$$

where $r = \sigma_{CC}^{\bar{\nu}}/\sigma_{CC}^\nu$. In R^- many systematics cancel to first order, including the effects of the quark and antiquark seas for $u, d, s,$ and c. Charm production only enters through $d_{valence}$ (which is Cabbibo suppressed) and at high x; thus the error from the charm mass is greatly reduced. The cross section ratios can be written in terms of the effective neutrino-quark coupling parameters g_L^2 and g_R^2 as

$$R^\nu = g_L^2 + r g_R^2 \tag{23}$$

$$R^{\bar{\nu}} = g_L^2 + \frac{1}{r} g_R^2 \tag{24}$$

$$R^- = g_L^2 - g_R^2 = \rho^2 (\frac{1}{2} - \sin^2 \theta_W), \tag{25}$$

9

Source	Error	Reduction in NuSOnG
Statistics	0.00135	100 times the statistics
ν_e, $\bar{\nu}_e$ flux prediction	0.00039	see Sec. 3.3.6
Interaction vertex position	0.00030	Better detector segmentation and more sophisticated shower identification.
Shower length model	0.00027	Better segmentation and more sophisticated shower identification.
Counter efficiency and noise	0.00023	Better, Minos-style counter design
Energy Measurement	0.00018	Likely to be at a similar level.
Charm production, strange sea	0.00047	See Sec. 2.4.4
R_L	0.00032	Likely to be at a similar level.
$\sigma^{\bar{\nu}}/\sigma^{\nu}$	0.00022	See Sec. 2.4.5
Higher Twist	0.00014	Likely to be at a similar level.
Radiative Corrections	0.00011	Likely to be at a similar level.
Charm Sea	0.00010	Under study
Non-isoscalar target	0.00005	Glass is isoscalar

Table 1: Source and value of NuTeV error on $\sin^2\theta_W$, and reason why the error will be reduced in the PW-style analysis of NuSOnG.

in which

$$g_L^2 \quad = (2g_L^\nu g_L^u)^2 + (2g_L^\nu g_L^d)^2 \quad = \quad \rho^2(\frac{1}{2} - \sin^2\theta_W + \frac{5}{9}\sin^4\theta_W) \tag{26}$$

$$g_R^2 \quad = (2g_L^\nu g_R^u)^2 + (2g_L^\nu g_R^d)^2 \quad = \quad \rho^2(\frac{5}{9}\sin^4\theta_W). \tag{27}$$

NuTeV fit for R^ν and $R^{\bar{\nu}}$ simultaneously to extract $\sin^2\theta_W$, obtaining the value $\sin^2\theta_W = 0.2277 \pm 0.00162$. The goal of NuSOnG is to improve on this error by a factor of two. Table 1 lists the errors which NuTeV identified and indicates those for which NuSOnG expects improvement. Many of the largest experimental systematics of NuTeV came from the method of separating CC and NC events, which relied on length. NuSOnG will have a more sophisticated model for differentiating CC and NC events, using shower shape and identification of Michel-electron followers from low energy pion decays.

From Fig. 1, it is apparent that the NuTeV measurement is in agreement with past neutrino scattering results, although these have much larger errors. However, the NuTeV result is in disagreement with the global fits to the electroweak data which give a Standard Model value of $\sin^2\theta_W = 0.2227$ [4]. Expressed in terms of the couplings, NuTeV measures:

$$g_L^2 = 0.30005 \pm 0.00137 \tag{28}$$
$$g_R^2 = 0.03076 \pm 0.00110, \tag{29}$$

which can be compared to the Standard Model values of $g_L^2 = 0.3042$ and $g_R^2 = 0.0301$, respectively. Sec. 2.2 (below) considers possible sources for this disagreement, both within and outside the Standard Model.

10

2.1.2 NuSOnG and New Physics

NuSOnG will provide important probes of physics beyond the Standard Model distinct from and complementary to those of the LHC. NuSOnG will seek indirect evidence for new physics by addressing anomalies in the precision electroweak data, and by providing unique information about neutrino coupling to the Z. In addition, precision measurements from NuSOnG will help to disentangle the complicated set of observations that will be present at the LHC and, in doing so, elucidate the mechanism of electroweak symmetry breaking. NuSOnG and the LHC provide distinct probes of new physics because new physics enters collider and neutrino scattering processes differently: neutrino physics measures different combinations of couplings to light quarks; neutrino scattering probes new physics at space-like momentum transfer (versus the time-like scattering at colliders); and systematics are very different between low and high energy experiments. Finally, NuSOnG will directly search for new particles and interactions in the lepton sector that might be missed by the LHC and must otherwise await discovery by the ILC.

2.1.2.1 *New Physics Observed through Coupling to the Z*

NuSOnG is unique among experiments in its ability to address the nature of the neutrino couplings to the Z boson in the near future. In the Standard Model, the neutrino coupling to the Z- and W-bosons is purely left-handed. Indeed, the fact that the neutrino coupling to the W-boson and an electron is purely left-handed is, experimentally, a well-established fact (evidence includes precision measurements of pion and muon decay, nuclear processes, etc.). By contrast, the nature of the neutrino coupling to the Z boson is, experimentally, far from being precisely established [5].

The best measurement of the neutrino coupling to the Z-boson is provided by indirect measurements of the invisible Z-boson width at LEP. In units where the Standard Model neutrino–Z-boson couplings are $g_L^\nu = 0.5$, $g_R^\nu \equiv 0$, the LEP measurement [6] translates into $(g_L^\nu)^2 + (g_R^\nu)^2 = 0.2487 \pm 0.0010$. Note that this result places no meaningful bound on g_R^ν.

Precise, model-independent information on g_L^ν can be obtained by combining $\nu_\mu + e$ scattering data from CHARM II and LEP and SLD data. Assuming model-independent couplings of the fermions to the Z-boson, $\nu_\mu + e$ scattering measures $g_L^\nu = 2\rho$, while LEP and SLD measure the left and right-handed couplings of the electron to the Z. The CHARM II result translates into $|g_L^\nu| = 0.502 \pm 0.017$ [5], assuming that the charged-current weak interactions produce only left-handed neutrinos. In spite of the good precision of the CHARM II result (around 3.5%), a combination of all available data allows $|g_R^\nu/g_L^\nu| \sim 0.4$ at the two σ confidence level [5].

Significant improvement in our understanding of g_R^ν can only be obtained with more precise measurements of $\nu + e$ scattering, or with the advent of a new high intensity e^+e^- collider, such as the ILC. By combining ILC running at the Z-boson pole mass and at $\sqrt{s} = 170$ GeV, $|g_R^\nu/g_L^\nu| \lesssim 0.3$ could be constrained at the two σ level after analyzing $e^+e^- \to \gamma+$missing energy events [5].

At NuSOnG, we estimate that g_L^ν can be measured at around the 0.86% level. This estimate is obtained by combining the statistical uncertainty (20,000 $\nu + e$ elastic scattering events) with an estimated 0.5% systematic uncertainty from the flux estimate. Fig. 2 (left) depicts an estimate of how precisely g_R^ν could be constrained if the Nu-
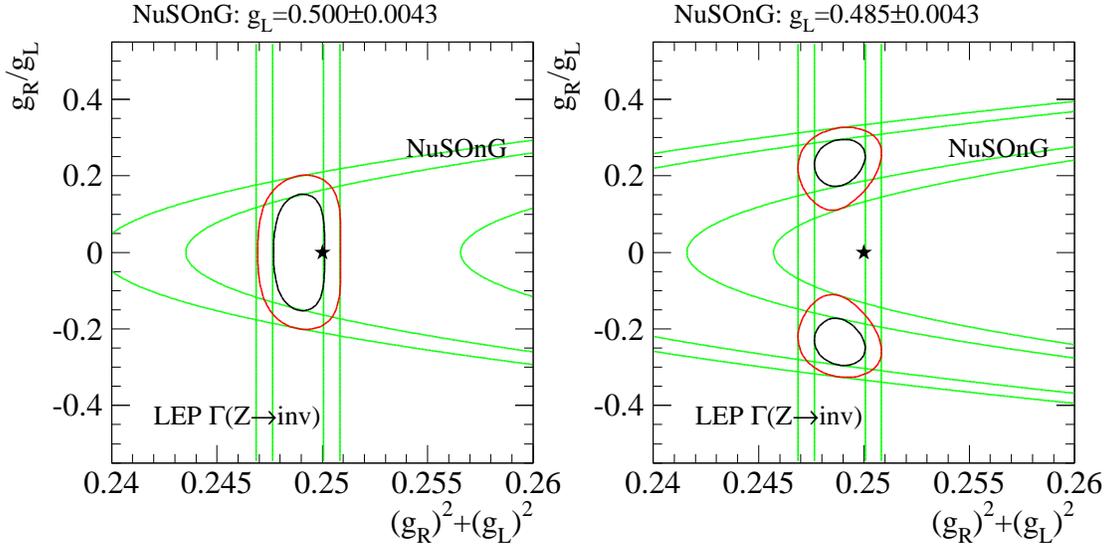
Figure 2: Precision with which the right-handed neutrino–Z-boson coupling can be determined by combining NuSOnG measurements of g_L^ν with the indirect determination of the invisible Z-boson width at LEP. In the left panel, we assume that the $\nu + e$ scattering measurement is consistent with the Standard Model prediction $g_L^\nu = 0.5$, while in the right panel we assume that the $\nu + e$ scattering measurement is significantly lower, $g_L^\nu = 0.485$, but still in agreement with the CHARM II measurement (at the one sigma level). Contours (black, red) are one and two sigma, respectively, while the star indicates the Standard Model expectation. See [5] for more details.

SOnG result, assumed to agree with the Standard Model prediction, is combined with the indirect LEP constraints. One can clearly see that this measurement ($|g_R^\nu/g_L^\nu| \lesssim 0.2$ at the two sigma level) compares favorably with the ILC capabilities described above. If the NuSOnG result is incompatible with Standard Model expectations but still in agreement with the CHARM II experiment, a combined NuSOnG–LEP analysis should be able to establish that $g_R^\nu \neq 0$, as depicted in Fig. 2 (right).

2.1.2.2 *New Physics Observed through Oblique Corrections*

Precision neutrino scattering measurements made at NuSOnG can reveal new physics even when new particles are not created in the final state, through the effects of these particles in loops. For models of new physics in which the dominant loop corrections are vacuum polarization corrections to the gauge boson propagators ("oblique" corrections), the ST parameterization introduced by Peskin and Takeuchi [7] provides a convenient framework in which to describe the effects of the new physics.

The ST parameterization begins with a reference Standard Model, including reference values for the Higgs and top masses, and predictions for observables in this reference Standard Model. Differences between predicted and experimental values of the observables are then parameterized by and used to fit for S and T, which can then be compared to predictions from new physics. The full set of precision electroweak data can then be used to constrain S and T, as shown in Fig. 3. The T parameter is
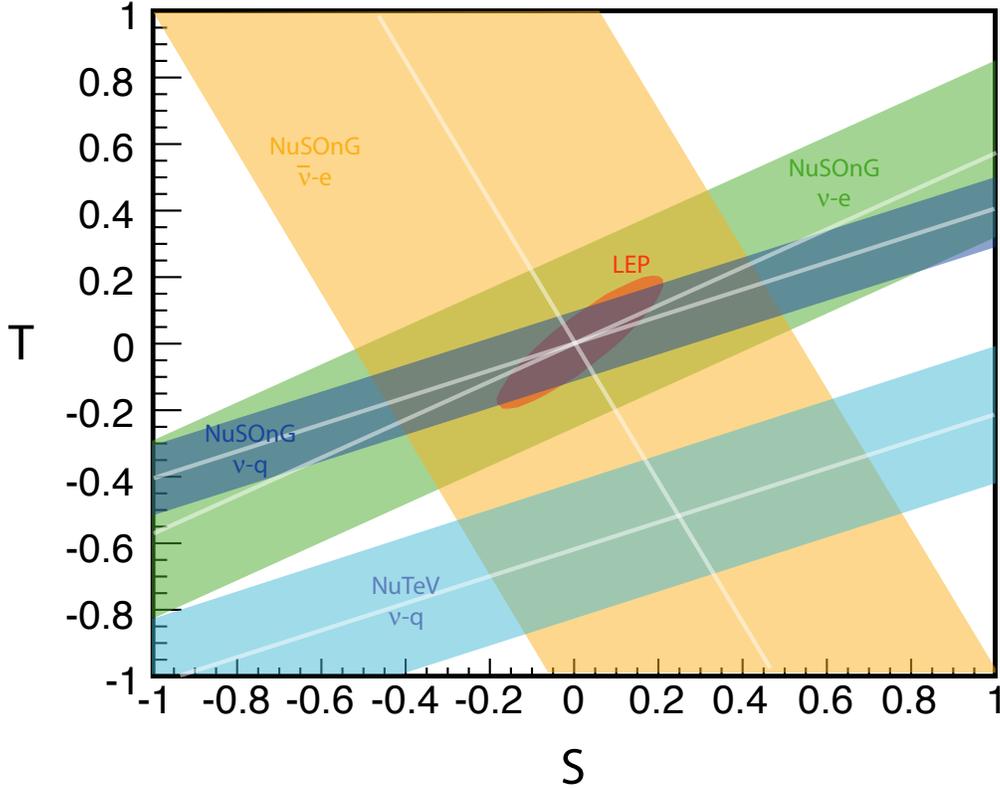
Figure 3: Three projected electroweak measurements from NuSOnG in S-T plane. LEP/SLD error ellipse is shown in red and the current NuTeV $\nu - q$ measurement is shown as a light blue band. The ochre band shows NuSOnG $\bar{\nu} - e$, the dark blue band shows NuSOnG $\nu - q$ and the green shows NuSOnG $\nu - e$. The width of the bands correspond to 68% confidence level for statistics as described in the text. The NuSOnG measurements assume $(S, T) = (0, 0)$.

sensitive to new physics that violates isospin and is zero for new physics that conserves isospin. Isospin-breaking new physics such as heavy non-degenerate fermion doublets or scalar multiplets would affect the T parameter. The S parameter is sensitive to isospin-conserving physics, such as heavy degenerate fermion doublets.

The status of electroweak measurements are shown in Fig. 3 [8]. The combined analysis of the LEP and SLD data by the LEP Electroweak Working Group (EWWG) [9] indicates an allowed region shown by the small oval, centered at $S = 0.05 \pm 0.10$ and $T = 0.07 \pm 0.11$. A different choice of reference Higgs or top mass changes Standard Model predictions for observables and thus shifts the center of the ST plot [10]; setting the Higgs mass to 1000 GeV would shift the center of the oval to roughly $(S, T) = (0.12, -0.36)$. Measurements of the W mass, which are not shown, are also consistent with the LEP measurements. The highest precision neutrino result comes from νq and $\bar{\nu} q$ scattering by the NuTeV experiment. This result clearly disagrees with the other

measurements, as discussed in Sec. 2.2.

The goal of NuSOnG is to make measurements which are competitive with or better than past electroweak measurements. These goals are indicated by the magenta ellipse and orange band on Fig. 3. The magenta ellipse shows the area in ST space which can be probed if a 0.7% measurement of the ν and $\bar{\nu}$ NC electron-scattering cross sections is achieved. The orange band shows the improvement in the neutrino-quark, "Paschos-Wolfenstein"-style measurement which is expected from NuSOnG.

Disregarding the NuTeV offset for the moment, one can now ask: how will this plot look in the era of LHC and what will NuSOnG add? We consider this question in light of three scenarios:

1. a light Higgs (115-200 GeV)

2. a heavy Higgs (200-1000 GeV)

3. no Higgs signal.

2.1.2.3 *NuSOnG Impact for a Light Higgs (115-200 GeV) Scenario*

A light Higgs is consistent with LEP/SLD and W mass data. The fit to the electroweak data excluding NuTeV indicates a mass less than 144 GeV at 95% CL. This is also consistent with the current best direct-search limit which finds $m_H > 114$ GeV [9]. In the case of the lightest Higgs masses, where the cleanest signal may be in $H \to \gamma\gamma$, a clear observation above background will be experimentally difficult and may take some time.

Once the LHC measurement of the Higgs mass is made, the center of the ST ellipse (Fig. 3) will be fixed at a point (modulo any remaining uncertainty in the top mass). Our experiment is especially interesting if the NuSOnG result disagrees with this LEP+SLD+LHC point. If the LHC measurement is high, *i.e.* $m_H \sim 200$ GeV, the result would be marginally inconsistent with the M_W analysis, which is 85^{+39}_{-28} GeV[9]. In this case, comparison with the ν_μ scattering results from NuSOnG could resolve the question of a discrepancy between these measurements.

If all other electroweak results are in good agreement, but disagree with NuSOnG, this would indicate new properties associated exclusively with the neutrino. An example would be decreased coupling of the neutrino to the Z boson, where suppression of the coupling comes from intergenerational mixing of the light neutrino with a moderately heavy neutrino:

$$\nu_\mu = (\cos\alpha)\nu_{\text{light}} + (\sin\alpha)\nu_{\text{heavy}}. \tag{30}$$

The $Z\nu_\mu\nu_\mu$ coupling is modified by $\cos^2\alpha$ and the $W\mu\nu_\mu$ coupling is modified by $\cos\alpha$. This model, inspired by the NuTeV anomaly (see Sec. 2.2), would yield a measurement in NuSOnG with a low NC-to-CC ratio in both the case of electron and quark scattering.

These moderately heavy right-handed states, dubbed "neutrissimos" [12], could have masses as low as just above the current bound of the Z mass. They may well be within the reach of the LHC and may appear as missing energy in events [12]. Some models allow for neutrissimos as light as ~ 100 GeV [13]. The neutrissimos decay very quickly, but not always invisibly. For example, in the reaction $N \to \ell + W$, the W may decay to either two jets or a neutrino–charged-lepton pair; only the latter case has missing energy. This may make recognition of the neutrissimo at LHC rather

14

difficult. In the case of $m_H < 130$ GeV, a dominant decay mode of the Higgs (along with $b\bar{b}$) could be into νN, where the neutrissimo subsequently decays. Reconstructing the Higgs in this case may be difficult at LHC; if neutrissimos exist, the result from NuSOnG may significantly improve our understanding of LHC results.

With a large tuning among the neutrino Yukawa couplings [13] neutrissimos could be the seesaw right-handed neutrinos. Relatively "large" mixing is marginally consistent with other constraints, including neutrinoless double-beta decay, which constrains $|U_{e4}|^2$ to be less than a few $\times 10^{-5}$ for a 100 GeV right-handed neutrino, and rare pion and tau decays, which constrain $|U_{\mu 4}|^2$ to be less than, most conservatively, 0.004 and $|U_{\tau 4}|^2$ to be less than 0.006. Other bounds come from $\mu \to e$ conversion in nuclei and other charged-lepton-flavor violation. A new experiment to search for $\mu \to e$ has been proposed at Fermilab [14] should also be sensitive to neutrissimos. The combination of NuSOnG and this experiment will be powerful in identifying the existence of these particles.

If the neutrissimo is a Majorana particle, it could be instrumental in elucidating the mechanism for leptogenesis. The present models of leptogenesis require very high mass scales for the neutral lepton, but theorists are pursuing ways to accommodate lower masses [15]. There also may be a wide mass spectrum for these particles, with one very heavy state required by standard leptogenesis models and others with masses in the range observable at LHC [16].

2.1.2.4 *NuSOnG Contribution in a Heavy Higgs (200−1000 GeV) Scenario*

While present electroweak data excluding NuTeV favor a light Higgs ($\lesssim 200$ GeV), as indicated in Fig. 3, the Higgs mass can extend up to about 1000 GeV without violating unitarity [17]. Thus, if LHC finds that the Higgs is between ∼200 and 1000 GeV and the LEP+SLD ellipse has no major systematic error, then new physics must explain the discrepancy. Candidate models of new physics may well affect the neutrino scattering and e^+e^- scattering differently, so the high-precision neutrino scattering measurements from NuSOnG will provide an important piece of the puzzle if the Higgs mass found at LHC is genuinely inconsistent with LEP+SLD predictions.

Introduction of a fourth family would compensate for a modestly heavy (∼ 300 GeV) Higgs by shifting the LEP+SLD allowed region back up in S and T [18]. This family would need to exist above the bounds of direct searches, which is $\gtrsim 300$ GeV. Mixing must be confined within the allowed bounds of the CKM matrix measurements [20]. A nice feature of this model is that a fourth-generation Majorana neutrino could play the role of dark matter. Depending on the underlying physics, evidence of a fourth family would be apparent in a shift of the NuSOnG result on the ST plot. This could be especially important if the physics introducing the fourth family is from a mechanism like "Top See Saw" [21], which will not be observable at LHC. The impact of this particular model on neutrino scattering is not yet thoroughly explored, but could prove interesting [22].

A classic method for masking a heavy Higgs is to introduce heavy Z bosons [23], which, as shown in ref. [10], tend to move the LEP-SLD ellipse upward in T, compensating for the heavy Higgs. Introduction of a $Z^{'}$ tends to increase NC rate in neutrino scattering and also to move the neutrino result upward on the ST plot (although with a different dependence than the LEP-SLD result).

15

There are good theoretical reasons for considering the existence of additional neutral heavy gauge bosons. Extra Z bosons appear in various GUT and string-motivated extensions to the Standard Model [24]. For example, the $E(6)$ breakdown to $SO(10) \times U(1)_\psi$ results in the Z_ψ. The $SO(10)$ break down to $SU(5) \times U(1)_\chi$ yields the Z_χ. Thus the new exchange boson could be: $Z' = Z_\chi cos\beta + Z_\psi sin\beta$, where the mixing angle β is an arbitrary parameter. Extra Z bosons also appear in other beyond Standard Model theories, including extra dimensions with gauge fields in the bulk [25]; little Higgs theories [26], which use heavy Zs to cancel divergences in the Higgs mass; and topcolor in which they drive electroweak symmetry breaking [27]. Heavy Zs provide a mechanism for new SUSY theories to evade the LEP bound of $m_H = 114$ GeV [28]. These models all produce new physics signatures at LHC. The precision measurement from NuSOnG can aid in differentiating models.

Models which introduce new physics to mask a heavy Higgs may seem contrived until one looks at the LEP+SLD data more closely. Up to this point we have considered the LEP+SLD measurements as a single result, however, many measurements enter this fit, and larger than expected inconsistencies between these measurements exist [29]. For example, there is a 3.2σ discrepancy between the forward-backward (A_{FB}) and left-right (A_{LR}) asymmetry measurements. Excluding the A_{FB} result, the LEP+SLD fit yields $m_H < 115$ GeV at 95%, with the best fit at 42 GeV – *i.e.* a range already excluded by direct searches, which require $m_H > 114$ GeV at 95% CL.

There are several ways to interpret this deviation. It may simply be that there are systematics involved in the A_{FB} measurement which have yet to be identified and which would bring this result into agreement with the others. In this case, we are in the dramatic situation of having already ruled out the Higgs. The scenario of no Higgs is considered in the next section. Alternatively, new physics is involved. This result is dominated by purely leptonic measurements. On the other hand, the fit to the hadronic asymmetries, dominated by A_{FB}^b has two χ^2 minima, at 450 and 3000 GeV. Thus, one may either introduce new physics which produces a 20% shift on A_{FB}^b alone; or introduce new physics which would indicate apparently low values of m_H in the lepton-based measurements, when actually the value is large. Within any of these scenarios, new precision results from NuSOnG will be valuable for understanding the underlying physics.

2.1.2.5 *NuSOnG and the Case of No Higgs*

Higgsless models do not employ the Higgs mechanism to render the Standard Model renormalizable [30]; instead they introduce some other scheme. The Higgs mechanism enforces unitarity in the scattering amplitudes of longitudinally polarized gauge bosons, $W_L^\pm + Z_L^o \to W_L^\pm Z_L^o$, for example. A requirement that the transition probability remains less than one gives the energy scale Λ at which a new mechanism must come into play,

$$\Lambda \sim \frac{4\pi M_W}{g} \sim 1.8 \text{TeV}. \tag{31}$$

Higgsless theories generally contain new mass bosons V_i with masses on the TeV scale that act to cancel the divergences in gauge boson scattering. Cancelling the amplitudes while respecting bounds from current electroweak couplings typically give small

couplings:

$$g_{WZV} < \frac{g_{wwz}M_Z^2}{\sqrt{3}M_1^{\pm}M_W} = 0.04 \tag{32}$$

for $M_1^{\pm}$=700 GeV.

At the LHC, the typical cross sections for V_i are hundreds of femtobarns, so, after cuts, the LHC experiments will record tens to hundreds of events in the first years of data taking. Since the V_i resonances serve the same purpose as the Higgs boson, additional information will be necessary to determine whether these resonances originate from spontaneous symmetry breaking or from strong coupling between the known gauge bosons. The electroweak measurements from NuSOnG will play a role in understanding the origin of such events, en route to a more complete explanation provided by the ILC.

2.2 The NuTeV Anomaly

The NuTeV anomaly is a 3σ deviation of $\sin^2\theta_W$ from the Standard Model prediction [4]. NuTeV employed the PW-inspired method discussed in Sec. 2.1.1.1, which resulted in a 0.75% measurement of the weak mixing angle (see Tab. 1). Two systematic adjustments to the NuTeV result have been identified since the result was published. The first is the new measurement of the K_{e3} branching ratio from KTeV, which does not significantly reduce the error, but introduces a correction moving the result away from the Standard Model. The second is the final measurement of the difference between the strange and antistrange seas (called "the strange sea asymmetry", see Sec. 2.4.4), which will pull the NuTeV result toward the Standard Model. A new analysis of the NuTeV data which will include these two corrections is expected be available in late summer, 2007 [32]. It should be noted that while an error from the strange sea appeared in the NuTeV analysis, no error on a strange sea *asymmetry* appeared in the original NuTeV analysis; this will be included in the upcoming re-analysis.

NuTeV is one of a set of $Q^2 \ll m_Z^2$ experiments measuring $\sin^2\theta_W$. It was performed at $Q^2 = 1$ to 140 GeV^2, $\langle Q_\nu^2 \rangle = 26$ GeV^2, $\langle Q_{\bar\nu}^2 \rangle = 15$ GeV^2, which is also the expected range for NuSOnG. Two other precision low Q^2 measurements are from atomic parity violation[34] (APV), which samples $Q^2 \sim 0$; and SLAC E158, a Møller scattering experiment at average $Q^2 = 0.026$ GeV^2 [35]. Using the measurements at the Z-pole with $Q^2 = M_z^2$ to fix the value of $\sin^2\theta_W$, and evolving to low Q^2, Fig. 4, from ref. [31], shows that APV and SLAC E158 are in agreement with the Standard Model. However, the radiative corrections to neutrino interactions allow sensitivity to high-mass particles which are complementary to the APV and Møller-scattering corrections. Thus, these results may not be in conflict with NuTeV. The NuSOnG measurement will provide valuable additional information on this question.

Since the NuTeV result was published, more than 300 papers have been written which cite this result. Various Beyond-the-Standard-Model explanations have been put forward; those which best explain the result require a follow-up experiment which probes the neutral weak couplings specifically with neutrinos, such as NuSOnG. Several "within-Standard-Model" explanations have also been put forward, based on the inherent issues involving scattering off quarks. NuSOnG can address these criticisms in two ways. First, we will provide better constraints of the quark-related distributions at issue. Second, we perform the measurement of the weak mixing angle in both a
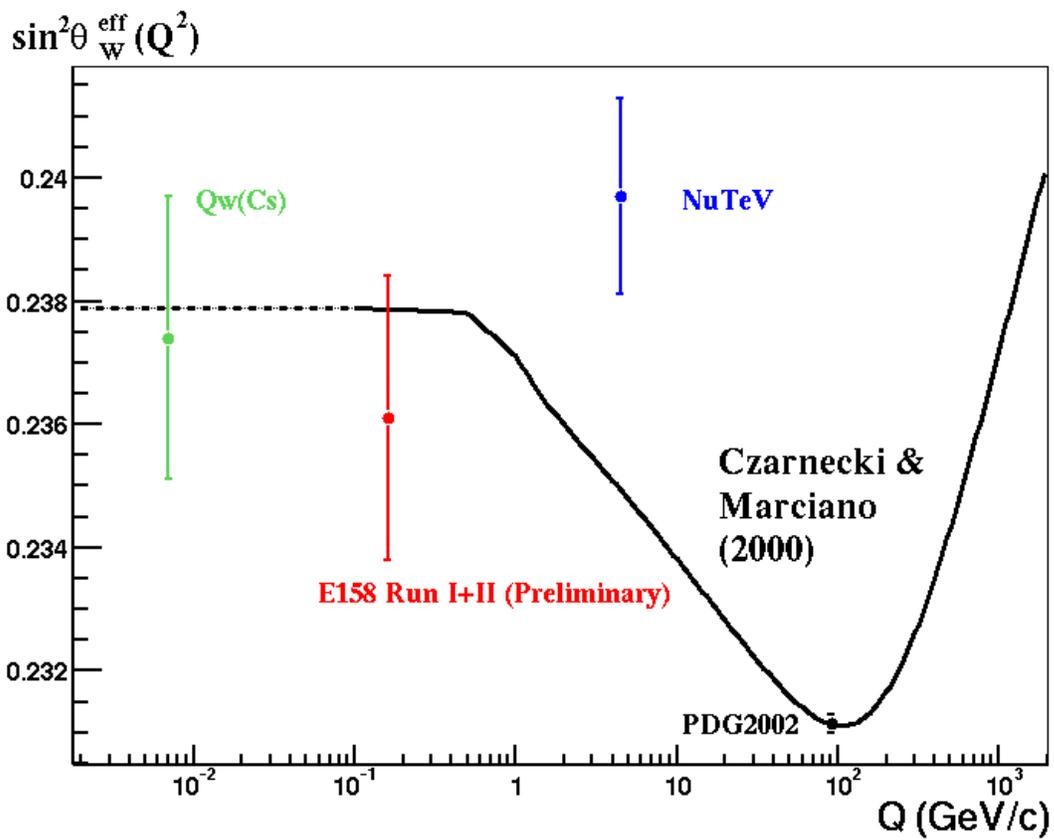
17

Figure 4: Measurements of $\sin^2\theta_W$ as a function of Q; from ref. [31]. The curve shows the Standard Model expectation.

purely leptonic mode (scattering from electrons) and via the PW method. Agreement between the two results would address the questions which have been raised.

2.2.1 Explanations Within the Standard Model

Four explanations for the NuTeV anomaly that are "within the Standard Model" have been proposed. These are: electromagnetic radiative corrections; higher order QCD corrections; isospin (or charge symmetry) violation; and the strange sea asymmetry. The radiative corrections will be disregarded here, since the results of this paper [36] are not reproducible.

The effect of the possible explanations is illustrated in Fig. 5. On this plot, the solid horizontal line indicates the deviation of NuTeV from the Standard Model. The thick vertical lines, which emanate from the NuTeV deviation, show the range of pulls estimated for each explanation, as discussed below. The dashed horizontal line shows the estimated shift due the new K_{e3} branching ratio. We do not yet have an estimated shift due to the new NuTeV strange sea measurement, but it is expected that this will move the dashed line toward the Standard Model [32].

Three "Standard Model" explanations may be considered next [37, 38]. First, the NuTeV analysis was not performed at a full NLO level; NuSOnG will need to undertake a full NLO analysis. But the effect of going to NLO on NuTeV can be estimated [39], and the expected pull is away from the Standard Model, as shown on Fig. 5. Second, the NuTeV analysis assumed isospin symmetry, that is, $u(x)^p = d(x)^n$ and $d(x)^p = u(x)^n$. Isospin violation can come about from a variety of sources and is interesting in its own right. NuSOnG's contribution to this study is discussed in Section 2.4.3. Various models for isospin violation have been studied and their pulls range from less than 1σ away from the Standard Model to $\sim 1\sigma$ toward the Standard Model [40]. We have chosen three examples [40] for illustration on Fig. 5: the full bag model, the meson cloud model, and the isospin QED model. These are mutually exclusive models, so only one of these can affect the NuTeV anomaly. Third, variations in the predicted strange sea asymmetry can either pull the result toward or away from the Standard Model expectation [41, 42, 43]. This issue is considered in detail in Sec. 2.4.4.

2.2.2 Beyond Standard Model Interpretations

Chapter 14 of the APS Neutrino Study White Paper on Neutrino Theory [44] is dedicated to "the physics of NuTeV" and provides an excellent summary. The discussion presented here is drawn from this source.

The NuTeV measurements of R^ν and $R^{\bar\nu}$, the NC-to-CC cross sections, are low. If one is assumes that the Higgs is light, then this must be interpreted as Beyond-Standard-Model physics that suppresses the NC rate with respect to the CC rate. Two types of models produce this effect and remain consistent with the other electroweak measurements: 1) models which affect only the Z couplings, *e.g.*, the introduction of a heavy Z' boson which interferes with the Standard Model Z; or 2) models which affect only the neutrino couplings, *e.g.*, the introduction of moderate mass neutral heavy leptons which mix with the neutrino.

As discussed in Sec. 2.1.2.4, introduction of Z' bosons tend to increase the NC rate rather than suppress it. Thus there is only a small subset of models which produce the destructive interference needed to explain the NuTeV result. Models which introduce

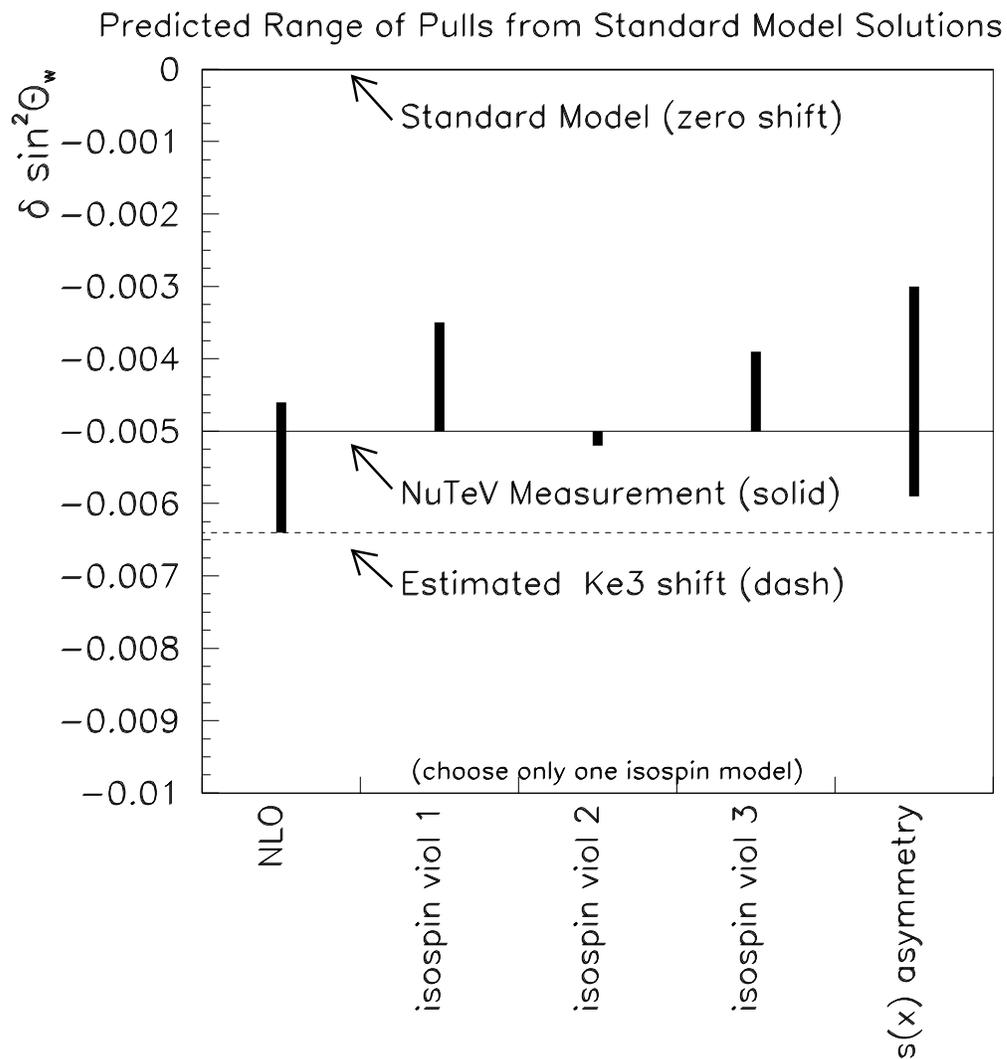Figure 5: Effect of various "Standard Model" explanations on the NuTeV anomaly. The y-axis is the deviation from the Standard Model. The solid line is the NuTeV deviation. The dashed line is an estimate of the effect of correcting for the new K_{e3} branching ratio. Thick black lines extending from the NuTeV deviation show the range of possible pulls from the various suggested sources, as described in the text.

a Z' which selectively suppresses neutrino scattering, without significantly affecting the other electroweak measurements, include cases where the Z' couples to $B - 3L_\mu$ [45] or to $L_\mu - L_\tau$ [46]. In the former case, fitting the NuTeV anomaly requires that $M_{Z'}/g_{Z'} \sim 3$ TeV. From the bounds from direct searches, this sets a limit on $M_{Z'} > 600$ GeV if the coupling is on the order of unity, but as low as 2 to 10 GeV if the coupling is $\sim 0.1\%$. The latter case is an example which improves the agreement between NuTeV and other results, but does not entirely address the problem. Its effectiveness in solving the NuTeV anomaly is limited by the data constraining lepton universality. This model addresses more than just the NuTeV anomaly. It is inspired by attempts to address bimaximal mixing in the neutrino sector. It has the nice features of also addressing the muon $(g - 2)$ measurement and producing a distinctive dimuon signature at LHC.

The case of models involving moderate-mass neutral heavy leptons, *a.k.a.* neutrissimos, have been discussed in the Sec. 2.1.2.3 and examples of viable models appear in ref. [11]. Eq. 30 described how the muon neutrino couplings might be modified by mixing. This idea can be extended to all three flavors, leading to a suppression factor for the Z coupling which is expressed as $(1 - \epsilon_\ell)$ and for the W by $(1 - \epsilon_\ell/2)$, where $\ell = e, \mu$, or τ. This addresses the NuTeV anomaly and at the same time suppresses the invisible width of the Z, describing the LEP I data.

If the NuTeV anomaly is due to Beyond Standard Model physics, then the effect will be visible in the neutrino-electron elastic scattering measurement also. Thus, if the NuTeV anomaly is borne out, NuSOnG would observe an ST plot similar to Fig. 6.

2.3 Direct Searches for New Physics

2.3.1 Light Neutrino Properties

Evidence for three light neutrino masses has now been established through neutrino oscillations in solar, atmospheric, and reactor experiments (see references [47] through [61]). Furthermore, although the MiniBooNE experiment recently refuted the LSND two-neutrino oscillation scenario at $\Delta m^2 \sim 1$ eV^2 [62], the question of the existence of multiple light sterile neutrinos still remains open [63]. These observations already require beyond-the-Standard-Model physics, and consequently raise phenomenological questions, such as: what are the mass and mixing parameters still allowed in sterile neutrino models? What do sterile neutrinos imply about neutrino mixing? Is the neutrino mixing matrix unitary, or is there effective freedom of mixing parameters? As we illustrate in the following sections, these are some of the questions that NuSOnG can potentially address.

2.3.1.1 *Matrix Freedom*

Perhaps the most interesting study of light neutrino properties which can be performed at NuSOnG is the search for evidence of "matrix freedom" or "nonunitarity." For example, in the case of existence of sterile neutrinos, the neutrino mixing matrix is extended to an $N \times N$ matrix, where $N > 3$. Under that assumption, it has been suggested that the $3{\times}3$ part of the matrix describing the three active (SM) neutrinos is not necessarily unitary; or, equivalently, the three flavor eigenstates are non-orthogonal (the $3{\times}3$ neutrino mixing matrix is *free*) [64].
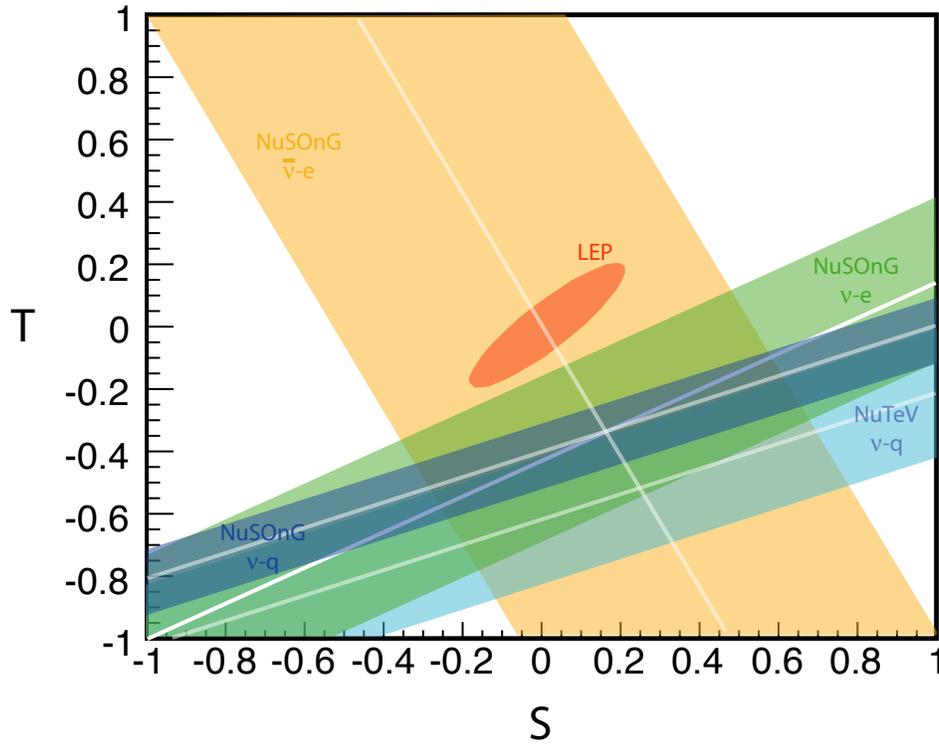
Figure 6: Three projected electroweak measurements from NuSOnG in S-T plane for a model model with a heavy Higgs inspired by the NuTeV measurement [11]. In this model, $(S, T) = (0.12, -0.36)$. The labeling is as in Fig. 3.

This introduces striking changes to the probability formula for neutrino flavor transitions. Assuming unitarity, the survival probability formula for a neutrino produced as flavor α is

$$P_{\alpha\alpha}^{unitary} = 1 - 4|U_{\alpha3}|^2[1 - |U_{\alpha3}|^2]\sin^2\Delta_{31}, \qquad (33)$$

where one has made use of $\Delta_{31} = \Delta m_{31}^2 \frac{L}{4E}$, and $\Delta m_{21}^2 \frac{L}{4E} \ll 1$. In the case of matrix freedom, the mixing matrix is no longer unitary. The level at which unitarity is violated can be defined as X_α, where

$$\sum_j |U_{\alpha j}|^2 = 1 - X_\alpha, \qquad (34)$$

with X_α being small. Under that assumption, the survival probability formula is then found to be

$$P_{\alpha\alpha}^{general} = P_{\alpha\alpha}^{unitary} - 2X_\alpha[1 - 2|U_{\alpha3}|^2\sin^2\Delta_{31}] + X_\alpha^2. \qquad (35)$$

As implied by Eq. 35 one of the main consequences of such scenario is instantaneous ($L = 0$) flavor transitions in a neutrino beam. This occurs regardless of the size of the mass splitting between the mostly sterile and mostly active states, and thus allows for a full-mass-range search for evidence of sterile neutrinos. A recent study [65] suggests that current experimental data limit such an effect to up to the order of a few percent.

As a result, several interesting and potentially observable phenomena can occur. Extending the argument of ref. [65], for instance, the non-orthogonality of ν_μ and ν_e that matrix freedom introduces, results in an instantaeous transition at $L = 0$ from ν_μ to ν_e [64]. Thus one could observe an excess of ν_e events in a pure ν_μ beam.

The trick to searching for this instantaneous transition is to focus on an energy range where the ν_e background is low and well constrained. In the case of NuSOnG, this is on the high energy tail of the flux, above $E \gtrsim 250$ GeV. For the limits on ν_μ transformation to ν_e[65], which are at the $\sim 1 \times 10^{-4}$ level, NuSOnG would see an excess of ~ 200 ν_e events in this high energy region. Fig. 7 shows the ratio of ν_e flux with ν_μ transitions to ν_e flux without transitions. The abrupt cutoff is due to Monte Carlo statistics; higher energies can be explored. Assuming that such transitions indeed happen at the 10^{-4} level, one would expect up to a 10% increase in flux for $E \sim 350$ GeV. In that high energy region, the ν_e flux is mainly from K^+ decay, which is well constrained by the ν_μ events. Such an excess should therefore be measurable.

Other interesting effects of matrix freedom [64] include the oscillatory behavior in the total (flavor-summed) CC event rate as a function of L/E, and (fake) CP-violating effects in the ν and $\bar{\nu}$ neutral-current event rates (the two rates oscillate differently with L/E). Potential observation of those effects at NuSOnG has not been explicitly considered at this stage, although it would be interesting to address this and we are planning to do so in the near future. Regardless of that, evidence of ν_e contamination in a ν_μ beam above expected background levels, something for which NuSOnG can search, would strongly support the matrix freedom hypothesis.

2.3.1.2   *Sterile Neutrino Oscillations*

Direct observation of sterile neutrino oscillations may also be possible in NuSOnG, depending on the mass and mixing parameters. Oscillations of active to light sterile neutrinos have been introduced to explain the LSND anomaly, as dark matter candidates, and in describing the supernova collapse models. These ideas span a wide
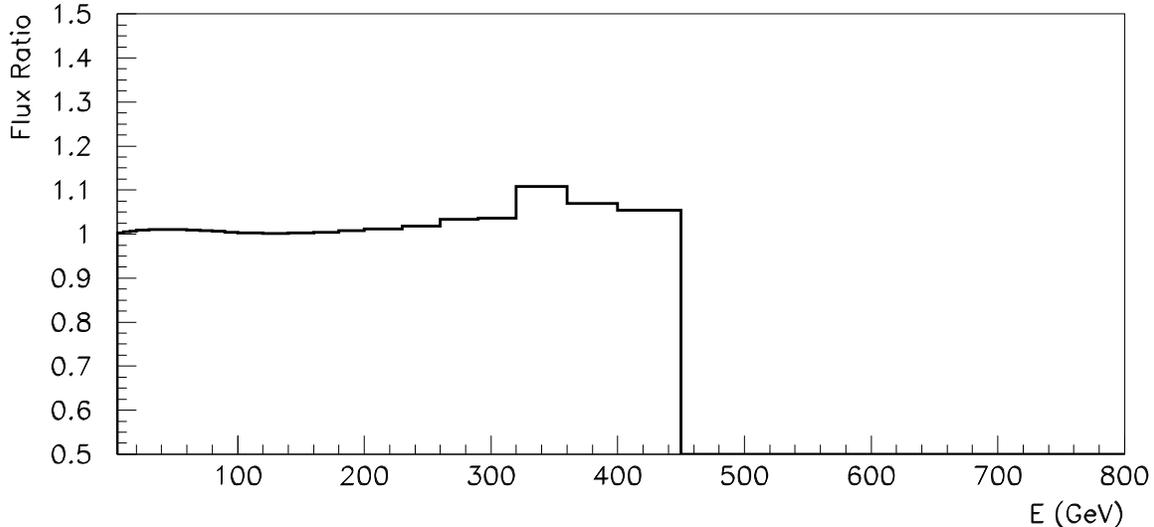
23

Figure 7: Ratio of enhanced ν_e flux due to ν_μ transitions to ν_e flux assuming no transitions. Obtained assuming 100M ν_μ deep inelastic scattering events.

range of Δm^2 values. The LSND anomaly requires a sterile neutrino in the range of ~ 1 eV^2 with moderate mixing ($\lesssim 1\%$), while dark matter candidates and supernova collapse models require ($\gtrsim 1$ keV)^2. These models also require tiny mixing ($10^{-13} < \sin^2 2\theta < 10^{-7}$)[66]. NuSOnG probes an intermediate range of Δm^2, between the LSND and astrophysical allowed regions. However, since sterile neutrinos may come in families, it is worth exploring this previously uncharted territory.

The NuSOnG experimental design consists of a 30-600 GeV muon neutrino beam, peaked at $\sim$100 GeV, incident on a $\sim$ 200-meter long detector located at L$\sim$1.5km from the neutrino source. This detector design allows for ν_μ disappearance studies across the detector length by examining the ν_μ scattering rate variation across the detector. Such searches would be limited by the detector energy resolution. Preliminary studies have shown that, assuming a 10% energy resolution, $\Delta m^2 \sim 600$eV^2 regions with mixing of $\lesssim 0.1$ can be probed easily. NuSOnG may also be able to explore smaller mixings and higher Δm^2s, depending on the final experimental design.

NuSOnG can also probe for ν_μ and ν_e disappearance in the range of $L/E = $ (1.5km/100 GeV) = 0.015, thus in the range of $\Delta m^2 \sim 50$ eV^2. This is a range which has been covered by past experiments including CCFR [67], CHDS [68], and NOMAD [69]. However, the improved quality of the first principles prediction due to the new SPY secondary production data [70], discussed in sec. 3.3, should allow improvement of these limits.

2.3.2 New Interactions

2.3.2.1 *Lepton Number Violation Searches*

The NuSOnG experiment possesses two valuable characteristics for the search for lepton number violation. First, it relies upon a high purity, high intensity beam as

its source of neutrinos; secondly, it employs an instrumented detector optimized to measure inverse muon decay with high accuracy. An experiment with these two features naturally lends itself to searches for the process:

$$\bar{\nu}_\mu + e^- \to \mu^- + \bar{\nu}_e. \tag{36}$$

This interaction is forbidden by the Standard Model since it violates lepton family number conversation ($\Delta L_e = -\Delta L_\mu = 2$). As such, observation of this reaction would immediately constitute direct observation of physics beyond the Standard Model.

A number of theories beyond the Standard Model predict that lepton number is not a true conserved quantum number; this means that processes that violate lepton number are allowed to occur. Theories which incorporate multiplicative lepton number conservation [71, 72], left-right symmetry [73], or the existence of bileptons [74] fall under this category.

The differential cross-section for lepton-violating processes can be parametrized in the following form:

$$\frac{d\sigma}{dy} = \lambda \frac{G_F^2 s}{\pi} (A_V \cdot y(y-r) + A_S \cdot (1-r)), \tag{37}$$

where y is the fractional energy carried by the outgoing lepton, G_F the weak coupling constant, s the square of the center of mass energy of the system, and r the threshold factor, defined as m_μ^2/s. The parameters λ, A_V, and A_S describe the strength of the reaction and whether the process is vector or scalar in nature. It is typical to compare this process to that of inverse muon decay:

$$\frac{\sigma(\bar{\nu}_\mu e^- \to \mu^- \bar{\nu}_e)}{\sigma(\nu_\mu e^- \to \mu^- \nu_e)} = \lambda \cdot (A_V \cdot (\frac{1 + r/2}{3}) + A_S). \tag{38}$$

The signature for such a reaction is the tagging of an μ^- during antineutrino running with the same signature as expected from inverse muon decays. The main backgrounds to this reaction include (a) ν_μ contamination, (b) ν_e contamination, and (c) charge misidentification of candidate events. Our current estimates place a very small beam contamination during antineutrino running: about 0.4% contamination of ν_μs and a 2.3% contamination of ν_e and $\bar{\nu}_e$ neutrinos (See Sec. 3.1). Charge misidentification is expected to be very small, on the order of 10^{-5}. If we assume a conservative knowledge of the backgrounds at the 5% level, this would imply a limit on the lepton number violation cross-section ratio of better than 0.2% (at 90% C.L.) for V-A couplings and less than 0.06% for scalar couplings. Previous searches, based on 1.6×10^{18} protons on target and smaller target masses, have placed limits on this cross-section ratio to less than 1.7% at 90% C.L. for V-A couplings and less than 0.6% for scalar couplings [75]. The NuSOnG experiment can therefore reach an improvement of over an order of magnitude compared to previous searches. This limit can be improved if further selection criteria are used in removing unwanted beam impurities or the quasi-elastic background contamination.

2.3.2.2   *Inverse Muon Decay*

The study of inverse muon decay, $\nu_\mu + e^- \to \mu^- + \nu_e$ provides access to the helicity structure of the weak interaction distinct from muon decay experiments. The weak

interaction polarizes the incident ν_μ, making inverse muon decay an excellent place to study departures from $V - A$ couplings. For inverse muon decay, $\sigma \propto (g_L^{V,e} g_L^{V,\mu})^2 (1 - \epsilon)$ [76] where $\epsilon = h - (-1)$ and h is the helicity of the incident muon. Ref. [77] has measured $\epsilon < 4.1 \times 10^{-3}$ and the current limit on $g_{LL}^V = (g_L^{V,e} g_L^{V,\mu}) > 0.96$ [78]. For a measurement of the total cross section scaled to the predicted cross section, the uncertainty on the coupling is $g_{LL}^V = (1/2)\sigma_\sigma / \sigma_{SM}$.

For NuSOnG, we expect $> 200k$ inverse muon decay events, which would give a statistical uncertainty of 0.002 on g_{LL}^V. However, we will need to determine the neutrino flux. Taking the $\nu_\mu + e^- \to \nu_\mu + e^-$ cross section as *known* gives the neutrino flux to 0.7%. Since we plan to use the inverse muon decay events for determining the flux for the electroweak measurements, NuSOnG will need to measure the efficiency and fiducial volume for both processes to better than 0.7%. Combined with other systematics, we should be able to achieve an total uncertainty of about 1-2% on g_{LL}^V, an improvement by a factor of four.

The key background will come from CCQE events that have small hadronic energy. We expect our high granularity will allow us to keep the systematic error from this source well below 1%, but this needs study.

Obviously, the manner of analysis described above is somewhat questionable. Ultimately, one would want to carry out a combined analysis of both neutrino elastic scattering on electrons and quarks and of inverse muon decay in the context of a specific model which relates the charged and neutral current coupling constants. For such an analysis, 1-2% uncertainty should still be achievable.

2.3.3 New Particles

2.3.3.1 *Long-lived, Light Neutral Heavy Leptons*

Another interesting NuTeV result arose from the search for long-lived, light (< 15 GeV) neutral heavy leptons. This was performed in a helium-filled decay region located upstream of the calorimeter. In the mass region of 2.2-15 GeV, NuTeV has a small expected background (0.07 ± 0.01 events), but observed three events. All events had two muons originating from a vertex within the helium decay region and missing energy. [79].

Since publication in 2001, no widely accepted explanation has been found. In 2006, D0 published a search for a similar decay signature in proton-antiproton interactions [80]. No events were found and some production models were excluded. The most viable remaining model is by Dedes *et al.*, which hypothesizes that the events are from decay of long-lived neutralinos. These are produced in the NuTeV beam dump through B hadron decays [81]. No other experiment has been able to match NuTeV's running conditions to further explore this intriguing result.

NuSOnG can address the question by including a low-mass (helium-filled) decay region between the calorimeter segments. Assuming parameters similar to those of NuTeV (except for a 20-fold increase in the number of protons on target), NuSOnG would expect to see 60 events with an expected background of 1-2 events. The sensitivity would scale directly with the decay volume, so the increased length compared to NuTeV (26 $m \to \approx 40\ m$) would increase this to 90 signal events over a 2-3 event background. Observing no signal would finally settle this outstanding question.

These decay regions allow exploration for a signal from a beyond-the-Standard-Model particle in other decay modes as well; other interesting modes include $\mu\pi$, μe, $e\pi$ and ee. NuSOnG's sensitivity to other new particles is similarly improved over NuTeV by the increase in beam intensity and decay volume, allowing us to study new regions of phase space.

2.3.3.2   *Muonic Photons*

In the mid-1990's there was interest in searching for "leptonic photons" – massless vector particles that couple according to flavor. Electronic, muonic, and tauonic photons, γ_e, γ_μ, and γ_τ were introduced [82]. Production occurs in secondary meson decays such as $\pi \rightarrow \nu_\mu \mu \gamma_\mu$, and detection can proceed through $\gamma_\mu + Z \rightarrow \mu^+ + \mu^- + Z$, where Z is the charged nucleus. These events have small missing p_T compared to the "trident" background, $\nu + Z \rightarrow \nu + \mu^+ \mu^- + Z$. The search by CHARM II sets the best limit at 1.6×10^{-6} [83].

Since this time, neutrino oscillations have been confirmed (see references [47] through [61]). This complicates the theory of "muonic photons," since, in this case, lepton flavor-charge is not conserved. As pointed out in reference [82], a theory with a non-conserved charge cannot have massless vector particles and a Coulomb-like potential. It appears very difficult to evade this problem.

Nevertheless, NuSOnG should search for these events. With higher rate and better segmentation than CHARM II, NuSOnG should have sensitivity in the range of $\sim 10^{-7}$. A significant excess would be quite startling.

2.4   Measurement of Parton Distribution Functions

The Deeply Inelastic Scattering (DIS) process provides crucial information about the structure of the proton which is used to determine the Parton Distribution Functions (PDFs). For example, in the recent CTEQ6HQ analysis, DIS data accounted for more than two-thirds of the data points used in the analysis.[1] As such, the DIS measurements form the foundation for the many calculations which make use of the PDFs.

In the basic DIS process, leptons scatter from hadrons via the exchange of an intermediate vector boson: $\{\gamma, W^\pm, Z\}$. Different boson probes couple to the hadrons with different factors, and it is important to combine data from these different probes to separate the different flavor components in the hadron. Unfortunately, three of the four DIS probes $\{W^\pm, Z\}$ have a (relatively) large mass and couple only weakly; this introduces a number of complications:

- The statistics for these weak processes are limited as compared with the photon-exchange processes.

- To compensate for the weak cross section, typically heavy nuclear targets (*e.g.*, Fe and Pb) are used; this introduces nuclear corrections when the results are scaled from the heavy target back to proton or isoscalar targets.

The NuSOnG experiment will generate high statistics (> 100M DIS events) measurements on an intermediate atomic-weight nuclear target (SiO_2). This will provide

---

[1]Specifically, there were 1333 DIS data points used out of the 1925 total.[84]

precise information on the linear combinations of PDFs which couple to the weak charged currents $(W^\pm)$, which can significantly improve the parton distribution fits. In this section, we first introduce the basics of DIS and the connection to parton distribution functions. Then we concentrate on three aspects of parton distribution studies where NuSOnG can make a unique contribution to the physics:

- Improved understanding of nuclear effects in neutrino scattering.
- Study of Charge Symmetry Violation
- Measurement of the Strange Sea
- Measurement of σ^ν and $\sigma^{\bar{\nu}}$

The latter two items are directly relevant to the electroweak studies proposed for NuSOnG (see Sec. 2.2.1).

2.4.1 Deep Inelastic Scattering and Parton Distribution Functions

The differential cross section for neutrino DIS depends on three structure functions: F_2, xF_3 and R_L. It is given by:

$$
\frac{d^2\sigma^{\nu(\bar{\nu})N}}{dxdy} = \frac{G_F^2 M E_\nu}{\pi \left(1 + Q^2/M_W^2\right)^2}
$$
$$
\left[F_2^{\nu(\bar{\nu})N}(x, Q^2) \left(\frac{y^2 + (2Mxy/Q)^2}{2 + 2R_L^{\nu(\bar{\nu})N}(x, Q^2)} + 1 - y - \frac{Mxy}{2E_\nu} \right) \right.
$$
$$
\left. \pm xF_3^{\nu(\bar{\nu})N} y \left(1 - \frac{y}{2}\right) \right], \tag{39}
$$

where the $\pm$ is $+(-)$ for $\nu(\bar{\nu})$ scattering. In this equation, x is the Bjorken scaling variable, y the inelasticity, and Q^2 the squared four-momentum transfer.

The function $xF_3(x, Q^2)$ is unique to the DIS cross section for the weak interaction. It originates from the parity-violating term in the product of the leptonic and hadronic tensors. For an isoscalar target, in the quark-parton model,

$$
xF_3^{\nu N}(x) = x\left(u(x) + d(x) + 2s(x)\right. \tag{40}
$$
$$
\left. -\bar{u}(x) - \bar{d}(x) - 2\bar{c}(x)\right),
$$
$$
xF_3^{\bar{\nu} N}(x) = xF_3^{\nu N}(x) - 4x\left(s(x) - c(x)\right). \tag{41}
$$

Defining $xF_3 = \frac{1}{2}(xF_3^{\nu N} + xF_3^{\bar{\nu} N})$, at leading order in QCD,

$$
xF_{3,LO} = \sum_{i=u,d..} xq(x, Q^2) - x\bar{q}(x, Q^2). \tag{42}
$$

To the level that the sea quark distributions have the same x dependence, and thus cancel, xF_3 can be thought of as probing the valence quark distributions. The difference between the neutrino and antineutrino parity violating structure functions, $\Delta(xF_3) = xF_3^{\nu N} - xF_3^{\bar{\nu} N}$, probes the strange and charm seas.

Analogous functions for $F_2(x, Q^2)$ and $R_L(x, Q^2)$ appear in both the cross section for charged lepton (e or μ) DIS and the cross section for ν DIS. At leading order,

$$
F_{2,LO} = \sum_{i=u,d..} e^2(xq(x, Q^2) + x\bar{q}(x, Q^2)), \tag{43}
$$

where e is the charge associated with the interaction. In the weak interaction, this charge is unity. For charged-lepton scattering mediated by a virtual photon, the fractional electromagnetic charge of each quark flavor enters. Thus $F_2^{\nu N}$ and $F_2^{e(\mu)N}$ are analogous but not identical and comparison yields useful information about specific parton distributions [87]. $R_L(x, Q^2)$ is the longitudinal to transverse virtual boson absorption cross-section ratio. The best measurements for this come from charged lepton scattering rather than neutrino scattering. In the past, neutrino experiments have used the charged lepton fits to R_L as an input to the measurements of xF_3 and F_2[85]. This, however, is just a matter of the statistics needed for a global fit to all of the unknown structure functions in x and Q^2 bins [86]. With the high statistics of NuSOnG, precise measurement of R_L will be possible from neutrino scattering for the first time.

In addition to fitting to the inclusive DIS sample, neutrino scattering can also probe parton distributions through exclusive samples. A unique and important case is the measurement of the strange sea through opposite sign dimuon production. When the neutrino interacts with an s or d quark, it produces a charm quark that fragments into a charmed hadron. The charmed hadron's semileptonic decay (with branching ratio $B_c \sim 10\%$) produces a second muon of opposite sign from the first:

$$\nu_\mu \; + \; \text{N} \; \longrightarrow \; \mu^- \; + \; c \; + \; \text{X} \tag{44}$$
$$\hookrightarrow s \; + \; \mu^+ \; + \; \nu_\mu. \tag{45}$$

Similarly, with antineutrinos, the interaction is with an $\overline{s}$ or $\overline{d}$,

$$\overline{\nu}_\mu \; + \; \text{N} \; \longrightarrow \; \mu^+ \; + \; \overline{c} \; + \; \text{X} \tag{46}$$
$$\hookrightarrow \overline{s} + \; \mu^- \; + \; \overline{\nu}_\mu. \tag{47}$$

The opposite sign of the two muons can be determined for those events where both muons reach the toroid spectrometer. Study of these events as a function of the kinematic variables allows extraction of the strange sea, the charm quark mass, the charmed particle branching ratio (B_c), and the Cabibbo-Kobayashi-Maskaka matrix element, $|V_{cd}|$.

For a more in-depth review of precision measurement of parton distributions in neutrino scattering, see ref. [88].

2.4.2 Nuclear Effects

Historically, neutrino experiments have played a major role in expanding our understanding of parton distribution functions through high statistics experiments such as CCFR [85], NuTeV [89], and CHORUS [90]. However, the high statistics extract a price since the large event samples require the use of nuclear targets – iron in the case of both CCFR and NuTeV and lead in the case of the Chorus experiment. The problem is that if one wants to extract information on *nucleon* PDFs, then the effects of the nuclear targets must first be removed. NuSOnG can provide key measurements which will improve these corrections.

In the case of charged lepton deep inelastic scattering, there are data available from nuclear targets covering the range from deuterium through iron and beyond. Thus, it has been possible to perform detailed studies of the A-dependence as a function of x and Q^2 from both the cross section and the structure function F_2. Such is not the case

in ν and $\bar{\nu}$ interactions where the corrections can be different for both cross sections or, equivalently, for F_2 and xF_3. In this case one must rely on theoretical models of the nuclear corrections. This is an unsatisfactory situation since one is essentially measuring quantities sensitive to the convolution of the the desired PDFs and unknown – or model dependent – nuclear corrections.

It is important to address the question of nuclear effects in neutrino scattering so that the neutrino data can be used in fits without bringing in substantial uncertainties. For example, in a recent analysis [91] the impact of new neutrino data on global fits for PDFs was assessed. The conclusion reached in this analysis was that the uncertainties associated with nuclear corrections precluded using the neutrino data to constrain the nucleon PDFs. If this uncertainty is addressed, the neutrino data will be a powerful addition to these fits.

Furthermore, nuclear effects are interesting in their own right. Comparison of the charged and neutral lepton scattering data can provide clues to the sources of the major features which appear in nuclear effects: shadowing, antishadowing, and the EMC effect. There is phenomenological evidence which suggests that the nuclear corrections for the ν and $\bar{\nu}$ cross sections might be rather similar and, in both cases, somewhat smaller than the corresponding corrections in charged lepton deep inelastic scattering. These latter two observations differ from the pattern suggested by the theoretical model [92] for nuclear corrections used in the analysis.

Fig. 8 shows some results from Ref. [91] in the form of "data/theory" averaged over Q^2 and presented versus x. The results are from a global fit but are plotted *without* the model-dependent nuclear corrections which were used in the fits. What is striking is the similarity of the ν and $\bar{\nu}$ results, and the overall pattern of deviations, similar to that seen in charged lepton DIS, although the deviations from unity are somewhat smaller. It is interesting to note that there is no clear indication of the turnover at low x which is observed in charged lepton scattering, called shadowing. However, this may be due to kinematic limits of the measurements.

To make progress in understanding nuclear corrections in neutrino interactions, access to high-statistics data on a variety of nuclear targets will be essential. This will allow the A-dependence to be studied as a function of both x and Q^2, as has been done in charged lepton deep inelastic scattering. PDFs from global fits without the neutrino data can then be used to make predictions to be compared with the A-dependent ν and $\bar{\nu}$ cross sections, thereby allowing the nuclear corrections to be mapped out for comparison with theoretical models.

The primary target of NuSOnG will be SiO_2. However, we can address this issue by replacing a few slabs of glass with alternative target materials: C, Al, Fe, and Pb. This range of nuclear targets would both extend the results of Minerνa to the NuSOnG kinematic region, and provide a check (via the Fe target) against the NuTeV measurement.

Given the NuSOnG neutrino flux, we anticipate $58k$ ν-induced and $30k$ $\bar{\nu}$-induced CC DIS events per ton of material. A single ton would be sufficient to extract $F_2(x)$ and $xF_3(x)$ averaged over all Q^2; a single 5 m$\times$5 m$\times$2.54 cm slab of any of the above materials will weigh more than that. The use of additional slabs would permit further extraction of the structure functions into separate (x, Q^2) bins as was done in the NuTeV analysis, at the potential expense of complicating the shower energy resolution in the sub-detectors containing the alternative targets; this issue will be studied via
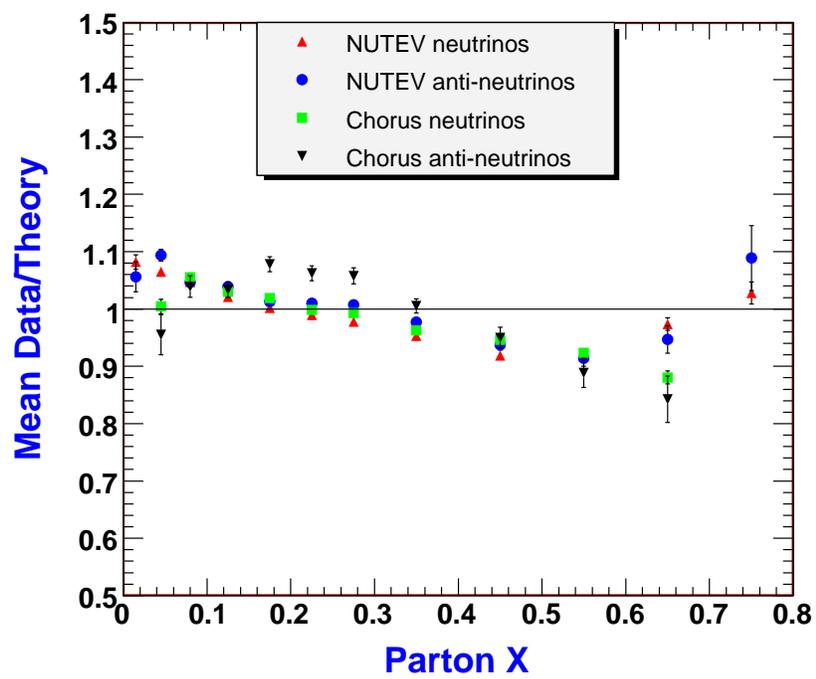
Figure 8: Comparison between the reference fit and the unshifted Chorus and NuTeV neutrino data without any nuclear corrections.

Material	Mass of 2.54 cm slab (tons)	Number of slabs needed for NuTeV-equivalent statistics
C	1.6	33
Al	1.9	27
Fe	5.5	10
Pb	7.9	7

Table 2: Alternative target materials for cross-section analysis

simulation.

Table 2 shows that two 50-module stacks would be sufficient to accumulate enough statistics on alternative nuclear targets for a full structure-function extraction for each material. However, for basic cross-section ratios in x, a single slab of each would suffice.

2.4.3 Isospin Violations

When we relate DIS measurements from heavy targets such as $^{56}_{26}$Fe or $^{207}_{82}$Pb back to a proton or isoscalar target, we generally make use of isospin symmetry where we assume that the proton and neutron PDFs can be related via a $u \leftrightarrow d$ interchange. While isospin symmetry is elegant and well-motivated, the validity of this exact charge symmetry must ultimately be established by experimental measurement. There have been a number of studies investigating isospin symmetry violation [93, 94, 95, 96]; therefore, it is important to be aware of the magnitude of potential violations of isospin symmetry and the consequences on the extracted PDF components. For example, the naive parton model relations are modified if we have a violation of exact $p \leftrightarrow n$ isospin-symmetry, (or charge symmetry); e.g., $u_n(x) \not\equiv d_p(x)$ and $u_p(x) \not\equiv d_n(x)$.

Combinations of structure functions can be particularly sensitive to isospin violations, and NuSOnG is well suited to measure some of these observables. For example, residual u, d-contributions to $\Delta x F_3 = x F_3^\nu - x F_3^{\bar\nu}$ from charge symmetry violation (CSV) would be amplified due to enhanced valence components $\{u_v(x), d_v(x)\}$, and because the $d \to u$ transitions are not subject to slow-rescaling corrections which strongly suppress the $s \to c$ contribution to $\Delta x F_3$. [95] Here the ability of NuSOnG to separately measure $x F_3^\nu$ and $x F_3^{\bar\nu}$ over a broad kinematic range will provide powerful constraints on the sensitive structure function combination $\Delta x F_3$.

There are a wide variety of models that study CSV [93, 94, 95, 96]. One method to quantify possible CSV contributions is via a one-parameter "toy" model where we characterize the CSV as a rotation in isospin space: $q_n^{\rm CSV} = N_q \sum_{q'} R_{qq'}(\theta) q'_p$, where R is a rotation matrix, and N_q is the normalization factor. For example, the u-distribution in the neutron can be related to the proton distributions via:

$$u_n^{\rm CSV}(x, Q^2) = N_u^2 \left[\cos^2(\theta) \, u_p(x, Q^2) + \sin^2(\theta) \, d_p(x, Q^2) \right] \quad . \tag{48}$$

For $\theta = \pi/2$, we recover the symmetric limit $u_p(x, Q^2) = d_n(x, Q^2)$. While this parameterization does not offer any explanation for the source of the CSV, it does provide a simple one-parameter (θ) characterization which is flexible enough to quantify the range of CSV effects. (For more details, cf. Ref. [95].)

At present, there are constraints on isospin violation from a number of experiments which cover different ranges of x and Q^2. For example, we note that while the above

"toy" model leaves the neutron singlet combination $(q + \bar{q})$ invariant at the $\lesssim 2\%$ level in the region $x \, \epsilon \, [0.01; 0.1]$, it would lower the NC observable $\left[\frac{4}{9}(u + \bar{u}) + \frac{1}{9}(d + \bar{d})\right]_n$ in this region by about 10%. An effect of this size would definitely be visible in the NMC F_2^n/F_2^p data which has an uncertainty of order a few percent.[87] The measurement of the lepton charge asymmetry in W decays from the Tevatron [97, 98] places tight constraints on the up and down quark distributions in the range $0.007 < x < 0.24$. While only strictly telling us about parton distributions in the proton, these data rule out isospin violations at the 5% level, as demonstrated in Ref. [98]. In addition, there are also fixed-target Drell-Yan experiments such as NA51 [99] and E866 [100] which precisely measure $\bar{d}/\bar{u}$ in the range $0.04 < x < 0.27$; these are also sensitive to isospin-violating effects.

NuSOnG will be able to provide high statistics DIS measurements across a wide x range. Because the target material (SiO_2) is very nearly isoscalar, this will essentially allow a direct extraction of the isoscalar observables. Consequently, if isospin violations are present, they can be measured more precisely than would be the case on a highly non-isoscalar target.

2.4.4 Measurement of the Strange Sea

There are several reasons why an improved measurement of the strange sea is of interest. First, it contributes to the low-Q^2 properties of the nucleon in the nonperturbative regime – a question of practical as well as intellectual interest, since many precision oscillation experiments are being performed in the 1 to 20 GeV (hence, nonperturbative) range. It is critical for charm production which provides an important testing ground for NLO QCD calculations. In addition, understanding the threshold behavior associated with the heavy charm mass is of interest to future neutrino experiments.

Distinguishing the difference between the $s(x)$ and $\bar{s}(x)$ distributions,

$$xs^-(x) \equiv xs(x) - x\bar{s}(x), \tag{49}$$

is even more important, and poses additional challenges. First, it is of intrinsic interest in nucleon structure models [43, 38, 37, 101, 102]. Second, the integrated strange sea asymmetry,

$$S^- \equiv \int_0^1 s^-(x)dx, \tag{50}$$

has important implications for the precision measurement of the weak mixing angle in deep inelastic scattering of neutrinos (*cf.* Sec. 2.2 and references [41, 43, 37, 38, 41, 101, 42]). This was not recognized at the time of the NuTeV $\sin^2\theta_W$ publication; an error due to S^- will be included in the NuTeV reanalysis, to be presented in late summer 2007 [32].

Historically, information on the $s(x)$ and $\bar{s}(x)$ distributions was derived from inclusive cross sections for neutral and charged current DIS via $\Delta(xF_3)$. These analyses made the implicit assumption that the $s(x)$ and $\bar{s}(x)$ seas had the same distribution in x. Because the strange sea is relatively small compared to the dominant $u(x)$ and $d(x)$ processes, the resulting uncertainties on the strange sea components were large. For example, the strangeness content of the nucleon, as measured by the momentum fraction carried by s or $\bar{s}$, is of order 3% at $Q = 1.5$ GeV. For this reason, the strange PDF was typically parametrized using the ansatz $s(x) = \bar{s}(x) = \kappa(\bar{u} + \bar{d})/2$, where κ measured the deviation from $SU(3)$ flavor symmetry at some low value of Q.
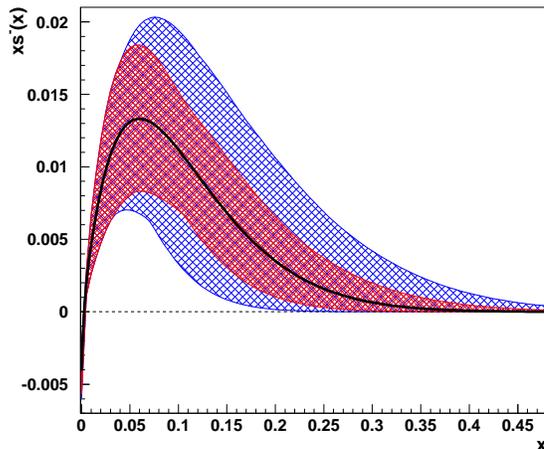
Figure 9: $xs^-(x)$ vs x at $Q^2 = 16$ GeV^2. Outer band is combined errors, inner band is without B_c uncertainty.

Introducing information from opposite sign dimuon production allows substantial improvement in the strange PDF measurement. Neutrino-induced dimuon production, $(\nu/\bar{\nu})N \to \mu^+\mu^- X$, proceeds primarily through the sub-processes $W^+ s \to c$ and $W^- \bar{s} \to \bar{c}$ (respectively), so this provides a mechanism to directly probe the $s(x)$ and $\bar{s}(x)$ distributions without being overwhelmed by the larger $u(x)$ and $d(x)$ distributions. Hence, the recent high-statistics dimuon measurements [103, 104, 105, 106, 107] play an essential role in constraining the strange component of the proton.

The highest precision study of s^- to date is from the NuTeV experiment [108]. The sign selected beam allowed measurement of the strange and antistrange seas independently, recording 5163 neutrino-induced dimuons, and 1380 antineutrino-induced dimuon events in its iron target. Figure 9 shows the measured asymmetry between the strange and antistrange seas. With more than 100 times the statistics of NuTeV, NuSOnG will have substantially finer binning.

The integrated strange sea asymmetry from NuTeV has a positive central value: 0.00196 ± 0.00046 (stat) ± 0.00045 (syst) $^{+0.00148}_{-0.00107}$ (external). The "external" error on the measurement is dominated by the error on the average charm semi-muonic branching ratio, B_c which is determined by other experiments. This error currently is about 10%. A rescan of Chorus data, which would increase the statistics, is under consideration [109].

The key to an improved result on the strange sea from NuSOnG is in a more precise measurement of B_c at NuSOnG energies. This can be accomplished in two ways. First, the very high statistics of NuSOnG allow for an accurate fit to B_c and the s and $\bar{s}$
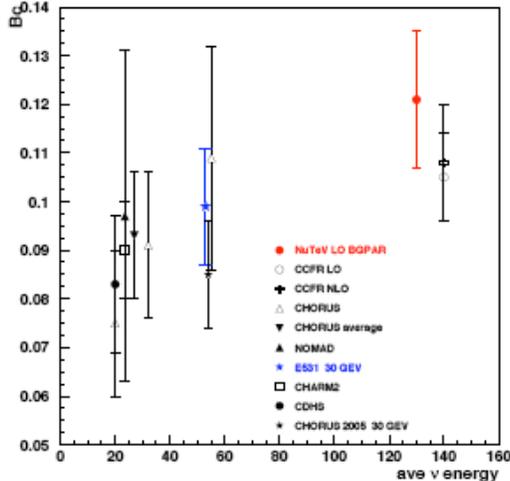
Figure 10: World measurements of B_c.

distributions simultaneously. Second, we plan to incorporate an emulsion detector into the design. The emulsion will be scanned by the Nagoya University group. This group has substantial expertise, having provided the emulsion and scanning for Chorus, DoNuT and other emulsion-based experiments. The goal will be to obtain $> 10k$ events in the emulsion during the NuSOnG run.

Beyond this, we will also consider placing a liquid argon TPC of similar size to microBooNE [110] (70 tons fiducial volume) or even Gargamelle (20 tons fiducial volume) in the gap between two of the NuSOnG subdetectors to directly measure B_c. If one were to, for example, use a volume comparable to the Gargamelle bubble chamber, we could observe on the order of one million charged current events within it for 5×10^{19} POT. This would yield approximately 100,000 events with charm in the final state, and about 10,000 dimuon events.

In addition to an improved measurement of B_c, the more finely-grained liquid argon TPC and/or emulsion detectors could be used to aid the calibration of the four glass detector modules by measuring any differences between hadron and electron showers from pion and electron beams versus those within a neutrino induced event. Coupled with the precision test beam, it may also be possible to improve understanding of the background due to muons produced by pion and kaon decays in the hadron shower. An improved parameterization of this background, currently from a CCFR measurement [111, 112, 113] could help extend the kinematic range of charmed dimuon measurements beyond what was possible for the NuTeV and CCFR experiments.

2.4.5   Measurement of the Total Cross Section

Precision measurement of the total neutrino and antineutrino cross sections at high energies will be valuable to a future neutrino factory experiment which seeks to make
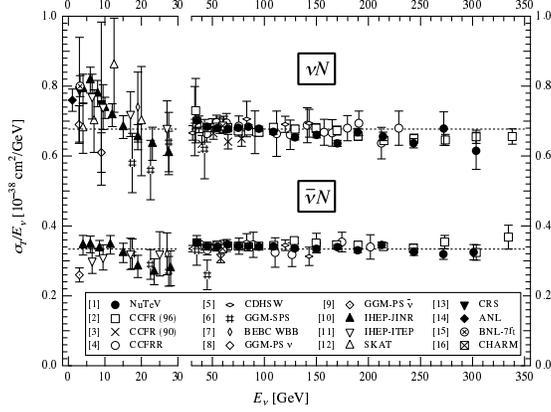
Figure 11: World measurements of the total ν and $\bar\nu$ cross sections. See references [89] and [114] through [128].

precision measurement of CP violation. Because NuSOnG can measure the flux to 0.5% (see Sec. 3.3, precise measurements can be made. Also, higher accuracy on the ratio of $\sigma^{\bar\nu}/\sigma^{\nu}$ will also improve the electroweak measurement (see Tab.1).

Fig. 11 shows σ/E_ν for the muon neutrino and antineutrino charged-current total cross-section as a function of neutrino energy ([89] and [114]-[128]). The error bars include both statistical and systematic errors. The results are from a wide range of target materials, but the experiments with the smallest errors and largest energy range used iron. The straight lines are the isoscalar-corrected total cross-section values averaged over 30-200 GeV as measured by the experiments in Refs. [115] to [117]. The fit [129] gives: $\sigma^{\nu\,Iso}/E_\nu = (0.677 \pm 0.014) \times 10^{-38} cm^2/GeV$; $\sigma^{\bar\nu\,Iso}/E_{\bar\nu} = (0.334 \pm 0.008) \times 10^{-38}$ cm^2/ GeV. The average ratio of the antineutrino to neutrino cross-section in the energy range 30-200 GeV is $\sigma^{\bar\nu\,Iso}/\sigma^{\nu\,Iso} = 0.504 \pm 0.003$ as measured by Refs. [89] and [114]-[117]. Note the change in the energy scale at 30 GeV.

The most precise measurements are systematics limited. The largest contributions to the systematics in recent experiments (CCFR, NuTeV) come from flux normalization, the model parameterization used in determination of the flux, and the charm mass used to parameterize charm threshold. NuSOnG measures the neutrino flux normalization to high precision via the IMD events. Also, as discussed in Sec. 3.3.2, NuSOnG's high statistics allow cuts which substantially improve the model parameterization error. Lastly, the charm mass, m_c is expected to be improved from the high statistics fits to the opposite sign dimuon events described in the previous section. While more study is needed, it likely that NuSOnG can substantially improve on the world measurements of the total cross section and the cross section ratios.
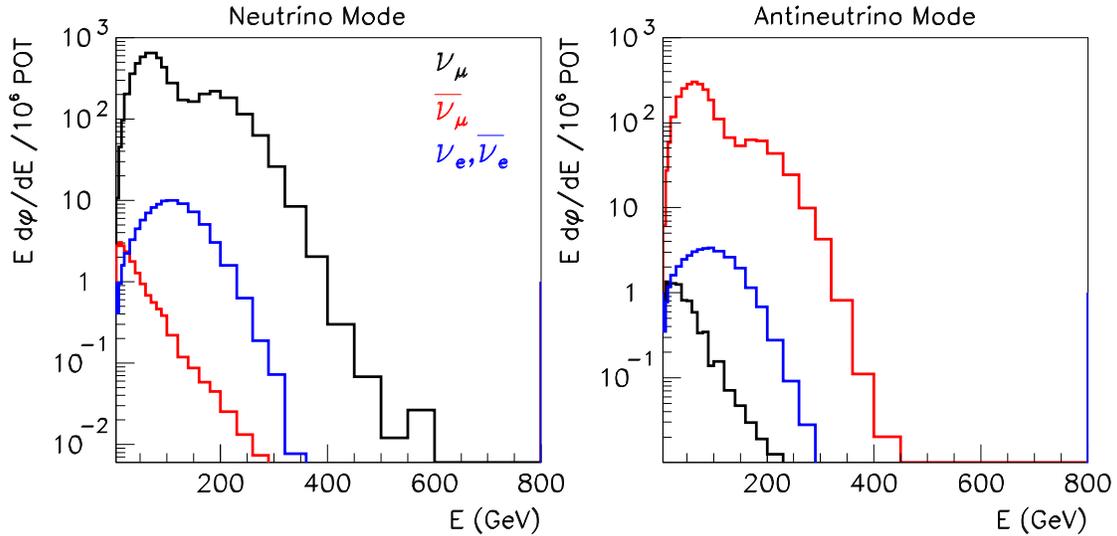
Figure 12: NuSOnG flux in neutrino mode (left) and antineutrino mode (right). Black: muon neutrino flux, red: muon antineutrino flux, blue: electron neutrino and antineutrino flux

3 Neutrino Flux and Event Rates

3.1 The Neutrino Flux

For the purposes of this expression of interest, we assume the same SSQT design as was used at NuTeV. The resulting neutrino (antineutrino) flux [33] is shown in Fig. 12, left (right). The ν_μ flux is shown in black, $\bar{\nu}_\mu$ in red, and $\nu_e + \bar{\nu}_e$ in blue. The shape of the flux is dominated by the dichromatic neutrino spectrum from π and K two-body decay.

In neutrino mode, 98.2% of neutrino interactions are due to π^+ and K^+ secondaries, while in antineutrino mode 97.3% come from π^- and K^-. The "wrong sign" content is very low, with an 0.03% antineutrino contamination in neutrino mode and 0.4% neutrino contamination in antineutrino mode. The electron-flavor content is 1.8% in neutrino mode and 2.3% in antineutrino mode. The major source of these neutrinos is

$K_{e3}^{\pm}$ decay, representing 1.7% of the total flux in neutrino mode, and 1.6% in antineutrino mode. Other contributions come from K_{Le3}, K_{Se3}, charmed meson, muon, Λ_C, Λ, and Σ decays.

Precise knowledge of the electron-flavor content is crucial for many NuSOnG analyses. The largest source of error in the knowledge of the electron-flavor content in NuTeV was from the $K_{e3}^{\pm}$ branching ratio, which led to an error on ν_e content of 1.4% [33]. While the other sources of ν_es have large fractional errors, they constitute a much smaller fraction of the flux. An error of 1.5% for the electron-flavor contamination, consistent with NuTeV, will be assumed for NuSOnG.

3.2   Event Rates

The *approximate* event rates presented here serve to set the scale for the physics case presented in this document. They are based on running the Nuance event generator [130] with the NuTeV flux, and then scaling to the expectations of NuSOnG assuming a 3 kton fiducial mass. Some simplifying assumptions, which will be corrected as the simulation develops, have been made. For example, C_2 is used as a target rather than SiO_2. Also, note that Nuance is not yet tuned as a high energy event generator. Thus, these event rates are only representative.

For neutrino running, approximate event rates for 5×10^{19} protons are:

507k	ν_μ CC quasi $-$ elastic scatters
178k	ν_μ NC $-$ elastic scatters
1016k	ν_μ CC π^+
302k	ν_μ CC π^0
272k	ν_μ NC π^0
226k	ν_μ NC $\pi^\pm$
1379k	ν_μ CC and NC Resonance multi $-$ pion
202M	ν_μ CC Deep Inelastic Scattering
63M	ν_μ NC Deep Inelastic Scattering
24k	ν_μ neutrino $-$ electron NC elastic scatters
235k	ν_μ neutrino $-$ electron CC quasielastic scatters(IMD)

For antineutrino running, which assumes 1.5×10^{20} protons on target, approximate event rates are:

548k	$\bar{\nu}_\mu$ CC quasi $-$ elastic scatters
195k	$\bar{\nu}_\mu$ NC $-$ elastic scatters
1103k	$\bar{\nu}_\mu$ CC π^+
321k	$\bar{\nu}_\mu$ CC π^0
297k	$\bar{\nu}_\mu$ NC π^0
246k	$\bar{\nu}_\mu$ NC $\pi^\pm$
1516k	$\bar{\nu}_\mu$ CC and NC Resonance multi $-$ pion
102M	$\bar{\nu}_\mu$ CC Deep Inelastic Scattering
36M	$\bar{\nu}_\mu$ NC Deep Inelastic Scattering

$21k$ $\quad$ $\bar{\nu}_\mu$ neutrino $-$ electron NC elastic scatters

$0k$ $\quad$ $\bar{\nu}_\mu$ neutrino $-$ electron CC quasielastic scatters (IMD)

The above were run for ν_μ and $\bar{\nu}_\mu$ beams. The relative ratios of event-weighted contents in neutrino mode are: $\nu_\mu - 98.33\%$, $\bar{\nu}_\mu - 0.08\%$, $\nu_e - 1.56\%$, $\bar{\nu}_e$ 0.03%. The relative ratios of event-weighted contents in antineutrino mode are: $\nu_\mu - 0.42\%$, $\bar{\nu}_\mu - 98.07\%$, $\nu_e - 0.26\%$, $\bar{\nu}_e$ 1.26%.

3.3 Precision Measurement of the Flux from Events in the Detector

Precise knowledge of the neutrino flux is key to many of the physics goals of the experiment. The goal, which is ambitious, will be to measure the neutrino flux as a function of energy to a precision better than 0.5%. This goal is a design-driver for the experiment. In this section, we outline an analysis plan to achieve this goal using the event types described in the previous section.

The flux will be determined through the following steps:

1. The inverse muon decay (IMD) events ($\nu_\mu + e^- \rightarrow \mu^- + \nu_e$) are, in principle, ideal for measuring the total flux because the IMD cross section is well known in the Standard Model. Therefore, these events will be used to determine the normalization of the flux. An important background to this measurement, however, comes from the CCQE events ($\nu_\mu + n \rightarrow \mu + p$), which must be subtracted. In this step, the predicted number of CCQE events is based on external cross section measurements. The error on the external cross section is likely to be the limiting systematic on the normalization determined in this step.

2. The shape of the flux is measured using the traditional "fixed ν" measurement method, which was applied in CCFR [85, 114]. and NuTeV [89], and is currently being used for in the Minos Experiment [131] to measure the shape of both the neutrino and antineutrino flux. The flux shape is then normalized by the IMD events from step 1 to obtain the initial flux prediction.

3. The initial flux prediction is used to determine a more precise CCQE cross section based on the NuSOnG data.

4. Step 1 is repeated using the more precise cross section determined in step 3. This produces the final normalization which is used to scale the results of step 2, yielding the final flux.

When the analysis is performed, it may be more effective and efficient to combine the above steps into a single multiparameter fit to the IMD and CCQE data, constrained by the external cross section information. However, for transparency we will consider the stepwise approach below.

Reaching the goal of $\lesssim 0.5\%$ systematic error depends mainly on the systematics of the IMD total event rate measurement. To set the scale of the problem, the best measurement of IMD events to date, from CHARM II, had a systematic error of 3% [132]. Thus, we must achieve an order of magnitude improvement in the IMD total systematic error. While we present a well-grounded back-of-the-envelope argument below, this level of measurement has yet to be demonstrated by simulation. That is a priority for future work on the development of NuSOnG.
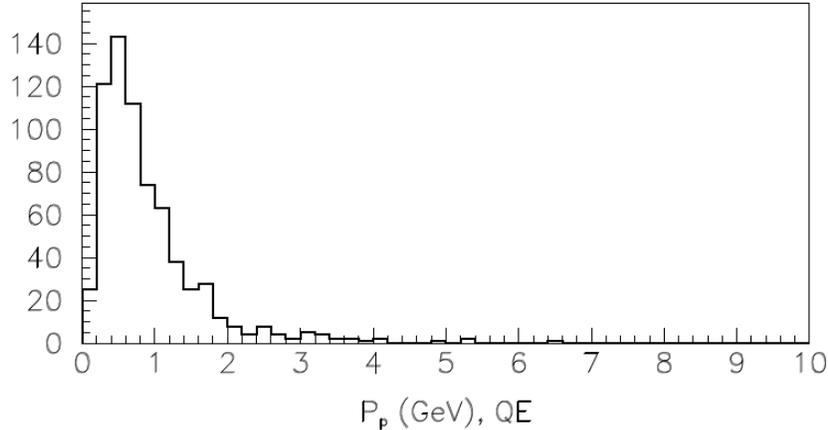
Figure 13: Momentum distribution of protons in ν CCQE events, from the Nuance Event generator.

Two useful cross checks of the measured NuSOnG flux are possible. First, one can extract an energy binned neutrino flux from the IMD events in step 1. Because of angular resolution, this flux may have substantial smearing, but it can be used as a compelling cross-check of the flux shape derived in step 2. Second, the neutrino to antineutrino flux ratio can be compared to the first principles prediction based on secondary production measurements.

3.3.1   Step 1: The IMD Measurement for Normalization

NuSOnG expects to observe $> 200k$ IMD events during neutrino running. The high statistics is a consequence of both the high neutrino flux and high neutrino energy. High energy is required because the threshold for IMD scattering is $E_\nu \geq E_\mu \geq \frac{m_\mu^2}{2m_e} = 10.9$ GeV. The SSQT beam design for NuSOnG produces minimal flux below 30 GeV, well within the range of IMD production. This indicates that there will be high statistics for IMD events in all flux bins.

These events will be used for total flux normalization, with the shape determined using the Fixed ν method described in step 2. This is done because, while these events can in principle be fully reconstructed assuming that the incoming neutrino enters parallel to the z-axis, the reconstruction in practice suffers substantial smearing. At ~ 100 GeV, IMD events will have scattering angles of $\lesssim 1$ mrad. This is similar in magnitude to the expected divergence of the beam, which was 0.62 mrad in NuTeV. Angular resolution errors are expected to be at a similar level.

IMD events must be separated from background, mainly due to CCQE-like interac-

tions (which include both real CCQE interactions and single π events where the pion was absorbed in the nucleus, and thus are effectively CCQE events). IMD events are qualitatively different from CCQE-like ones in two ways: there is no hadronic energy in the event, and there is a strict kinematic limit on the transverse momentum of the outgoing muon, $p_T \leq 2m_e E_\mu$. It is therefore crucial to design NuSOnG for observation of very low hadronic energy in the presence of a muon track, and for excellent angular resolution on the outgoing muon. The fine segmentation of NuSOnG should allow hadron identification in the presence of a muon to substantially lower energy (~ 0.75 GeV) compared to 1.5 GeV for Charm II [132] and 3 GeV for NuTeV[75]. One can see from the momentum distribution of the protons produced in CCQE interactions, shown in Fig. 13, that this approach will allow NuSOnG to cut more of the CCQE background than was possible in the previous experiments. NuSOnG also expects better IMD resolution than Charm II, due to the finer segmentation, which will reduce backgrounds.

Events which produce very low energy pions can also produce a background, although at a lower level than the CCQE background. NuSOnG's open trigger will allow many of the low multiplicity DIS events and $CC\pi^+$ events to be identified and cut due to the presence of subsequent michel electrons which come from the $\pi^+ \to \mu^+ \to e^+$ decay chain. A 50 MeV michel electron will traverse 12 cm of glass, producing hits in up to four chambers in the vicinity of the interaction vertex.

The IMD method for determining the flux proceeds in the following manner. After cutting on hadronic energy, minimum energy for the outgoing muon, and no michel electrons near the vertex, the plot of muon p_T will show a sharp peak at $p_T \sim 0$ superimposed on a broad continuum of background events extending to high p_T. The continuum is fit and extrapolated under the IMD peak, to extract the number of IMD events. This is divided by the theoretical cross section to yield the flux.

At the high energies of NuSOnG, the only nuclear effect expected for CCQE events comes from the Pauli exclusion effect. This produces an overall suppression of the cross section across all energies. Both the NuTeV and Charm II measurements suffered from the lack of availability of precise information on the Pauli exclusion effect. This resulted in an error on the Charm II measurement from the CCQE model of 2.1%.

NuSOnG will be in the fortunate position that a number of new measurements of the CCQE cross section on nuclear targets will be available as inputs into the CCQE model. Results from MiniBooNE [133] and SciBooNE [134] will address Pauli suppression in CCQE interactions on carbon. Minerva [135] is studying a series of nuclear targets, and are willing to consider running a glass target for NuSOnG, if we were to supply the target panels. The precision on the CCQE cross section in the NuSOnG era may be 5%, which is ~ 5 times better than the CHARM II era measurements. Thus, at this step, the CCQE model error for NuSOnG may be as low as 0.4%.

A CCQE model error which was not addressed in the Charm II analysis was the long-standing discrepancy between models and data at low Q^2 [133]. Low Q^2 events having small scattering angles represents a significant error on the extrapolation under the IMD peak. This discrepancy has recently been resolved by MiniBooNE under a dipole form-factor model [133]. Minerva plans to address the Q^2 dependence of the form factor in a model-independent way [136]. We will assume that the discrepancy will be fully addressed by the time of the NuSOnG run.

Another 1.5% systematic error in Charm II came from the model of the other sources

of low hadronic energy CC events, which are dominated by Δ resonant production. As described above, NuSOnG expects a substantially lower contamination from these sources because of the lower energy threshold and the michel electron veto. For those background events which are not cut, the modeling of these sources will substantially improved using Minerva data. In Minerva, the tracks from $CC\pi^+$ events are well reconstructed, so models p_T distribution of outgoing muons can be tuned. Similarly, Minerva offers the opportunity to accurately parametrize $CCpi^0$ events. Again, the total error on the low hadron multiplicity events in 2015 is expected to be on the order of 5%, so the modeling of these backgrounds should not be a limiting systematic.

IMD events can be cut from the sample due to electromagnetic radiation of the muon near the vertex region which is mistakenly identified as hadronic energy at the vertex. The NuTeV IMD analysis [75] assigned a 1% systematic error due to radiative effects. We address this error in two ways. First, in the NuTeV experiment, the photons immediately converted in the 10 cm iron plates, while in NuSOnG, the 2.5 cm glass plates are $0.25\lambda_0$, giving photons a 50% probability of traversing three plates before showering. Fewer IMD radiative events will therefore be misidentified as events with hadronic energy at the vertex. Second, because of the higher segmentation, NuSOnG will employ an improved model of electromagnetic showers, reducing the systematic error.

3.3.2 Step 2: The Fixed-ν Measurement to Determine the Shape

The central premise of the Fixed ν method for measuring the flux is that, for small hadronic energy exchange (ν), the differential cross section is independent of energy to a good approximation. The Fixed-ν method utilizes this fact to measure the relative flux between energy bins and the relative flux between neutrino and antineutrino interactions. External input is then needed to determine the overall normalization.

To motivate the premise, consider the differential cross section at a fixed ν integrated over all x:

$$\frac{d\sigma}{d\nu} = A(1 + \frac{B}{A}\frac{\nu}{E_\nu} - \frac{C}{A}\frac{\nu^2}{2E_\nu^2}). \tag{51}$$

In this equation,

$$A = k\int F_2(x, Q^2)dx, \tag{52}$$

$$B = -k\int [F_2(x, Q^2) \mp xF_3(x, Q^2)]dx, \tag{53}$$

$$C = B - k\int F_2(x, Q^2)(\frac{\frac{1+2Mx}{\nu}}{1 + R(x, Q^2)} - \frac{Mx}{\nu} - 1)dx, \tag{54}$$

$$\tag{55}$$

where $k = (G_F^2 M)/\pi$, and $\mp$ refers to neutrinos ($-$) or antineutrinos ($+$). For simplicity, first consider $\nu \to 0$. The cross section becomes equivalent to A, which is a constant. Since it is impossible to measure scattering for $\nu = 0$, consider scattering for $\nu = \nu_0$ where $\nu_0 \ll E_\nu$. As long as ν_0 is small enough, the terms which depend on ν_0/E_ν will have negligible contribution. Thus for a fixed, low value of ν, $d\sigma/d\nu \to A$, independent of beam energy. Note that terms B and C differ for neutrinos and antineutrinos. However, as long as ν_0/E_ν is negligible, these terms do not contribute and the cross section for antineutrinos is equal to the cross section for neutrinos.

42

From this, one can see how to measure the relative fluxes. If one measures the number of events at a given ν_0 in bins of E_ν, one can solve for the flux:

$$\Phi(E_\nu) = N(E_\nu, \nu_0)/A \quad . \tag{56}$$

The relative change of flux between two energy bins is independent of A:

$$\Phi(E_\nu^{bin1})/\Phi(E_\nu^{bin2}) = N^{bin1}(E_\nu, \nu_0)/N(E_\nu^{bin2}, \nu_0) \quad . \tag{57}$$

Since the neutrino and antineutrino cross sections are equal, this method also allows the relative fluxes to be extracted, independent of A.

$$\Phi(E_\nu)/\Phi(E_{\bar{\nu}}) = N(E_\nu, \nu_0)/N(E_{\bar{\nu}}, \nu_0) \quad . \tag{58}$$

Thus one can extract the relative bin-to-bin and neutrino-to-antineutrino fluxes strictly from the data, with no theoretical input on the value of A.

In practice one uses a low ν region, defined by $\nu < \nu_0$ where ν_0 is some appropriate upper limit. CCFR and NuTeV, used $\nu < \nu_0 = 20$ GeV, which allowed high statistical precision for the measurement. From the theoretical point of view, however, this was not optimal since the goal was to measure the flux down to $E_\nu = 30$ GeV, thus at $\nu = 20$ GeV, the ν/E_ν terms were not negligible. The flux is then given by:

$$\Phi(E_\nu) = \int_0^{\nu_0} \frac{\frac{dN}{d\nu}}{1 + \frac{B}{A}\frac{\nu}{E_\nu} - \frac{C}{A}\frac{\nu^2}{2E_\nu^2}} d\nu \quad . \tag{59}$$

A fit to $dN/d\nu$ determines B/A and C/A. One can test the quality of the bin-to-bin result by fitting σ/E to a line. A good fit results in small slope, due to QCD effects on the order of a few percent (somewhat smaller in antineutrino mode), with small error. NuTeV found values consistent with expectation [89]:

$$\frac{\Delta(\frac{\sigma^\nu}{E})}{\Delta E} = (-2.2 \pm 0.8)\%/100\text{GeV}, \tag{60}$$

$$\frac{\Delta(\frac{\sigma^{\bar{\nu}}}{E})}{\Delta E} = (-0.2 \pm 0.8)\%/100\text{GeV}. \tag{61}$$

The NuTeV analysis indicated a good fit to a straight line, as expected. The extracted shape of the flux was obtained to very high precision across the full energy range by this approach.

NuSOnG has an important advantage over NuTeV when implementing this method, in that the high statistics and good segmentation will all us to reduce this range of the low ν substantially, perhaps to as low as $\nu < \nu_0 = 10$ GeV. This should allow an even more precise measure of the shape than was obtained by past experiments, since the contribution of the fit to the B and C terms will be reduced. In particular, the systematic error contribution from the charm mass will be substantially reduced.

NuTeV also required $\nu > 5$ GeV to cut the resonance region. NuSOnG is also likely to introduce such a cut. However, this should be revisited in light of the expected new data from Minerva in the resonance region.

The most important detector systematic to this measurement is likely to be the muon energy scale. NuTeV achieved knowledge of the muon energy scale to 0.7%, although the absolute calibration beam was known to 0.3%. The difficulty was mapping

across the full area of the toroids. For NuSOnG to achieve its goal of measuring the flux with $\lesssim 0.5\%$ total error, the muon energy scale will need to be known to about 0.25%. Careful thought must be put in to understand how to achieve this.

In past experiments, the next step was to obtain the absolute flux by normalizing to the world's total, which is $\sigma/E_\nu = 0.667 \pm 0.014 \times 10^-38 cm^2/$GeV. It necessarily introduces a 2% normalization error into this method. NuSOnG will use the IMD events to perform the absolute normalization, rather than relying on the world average neutrino cross section measurement. This is done by scaling the total flux measured in neutrino mode with the Fixed ν method to $\sum_i N^{IMD}(E_i) \int \sigma^{IMD} dE$. At the end of this step, the predicted flux is expected to be known to $\sim 1\%$.

3.3.3 Step 3: A Precise Measurement of the CCQE Cross Section

At this point in the procedure, the limiting systematic is likely to be the CCQE cross section model error in the IMD normalization. In this step, this cross section is further constrained using the CCQE data in NuSOnG.

The background to the CCQE cross section analysis will be the low hadronic energy events. These can be reduced using the michel veto method discussed in Step 1. Beyond this, because CCQE scatters extend to higher angles, excess hits due to the presence of charged pions and photons from π^0 decay should be more easily resolved from the photon track. NuSOnG expects ~ 500k CCQE events, and thus stringent cuts can be applied to remove backgrounds without substantial statistical error, assuming the efficiency of the cuts can be well-understood.

The goal will be for NuSOnG to measure the CCQE cross section to $\lesssim 2\%$. This would be a very valuable measurement in its own right, as well as allowing for improvement in the flux extraction in the following steps. This result can be used to constrain the normalization for a glass-target measurement in Minerva. Ratios to the other nuclear target cross section measurements by Minerva then allow precisely determined measurements at low E across a wide range of nuclei. This will be useful input to future precision neutrino oscillation measurements.

3.3.4 Step 4: The Final NuSOnG Flux

Once the CCQE cross section has been determined at the $\lesssim 2\%$ level, one can iterate the IMD analysis of step 2 and then renormalize the distributions in step 3. The resulting flux is expected to have errors of $\lesssim 0.5\%$.

3.3.5 Cross Checks

Two useful cross checks of the flux are possible. The first takes the measured flux and compares it to the IMD event rate in energy bins. The second uses external data to cross check the shape and normalization of the antineutrino flux.

The first cross check compares the shape of the neutrino flux determined at step 1 to the shape determined through step 2. This will be done by running the final flux through the MC and using it to predict the IMD rate in energy bins. We will then extract the predicted flux in energy bins to compared to the measurement performed in step 1. This provides a powerful consistency check.

44

We can also cross check the fluxes obtained by the above method using a first-principles prediction based on external secondary production measurements. The absolute predictions in neutrino and antineutrino mode are unlikely to be an effective cross check because of large errors in the secondary production predictions, which vary from 5 to 10%. However, the prediction of the ratio of the neutrino to antineutrino fluxes may be possible to high precision. This requires some investigation.

Reference [139] provides a compendium of secondary production experiments in Table 3. None extend up to 800 GeV. The most relevant experiment was NA56/SPY at 450 GeV, which took data on beryllium targets[70]. This experiment published yields of π^+,π^-,K^+ and K^- with errors on each measurement of $\sim 5\%$. However, because many of the systematics cancel in ratio, the π^-/pi^+, K^-/K^+ and π/K ratios are each determined to $\sim 2.5\%$. This data should allow a good cross check of the individual π and K shape contributions. We may choose to run for a short period at 450 GeV in order to have an exact cross-comparison.

3.3.6   The Electron Neutrino Flux

We will begin by tuning the NuSOnG Beam Monte Carlo using the recent secondary meson production measurements described above. The new K production results will improve the first principles prediction for electron neutrinos beyond those of NuTeV. The electron neutrino contamination then can be further constrained through the precision measurement of the ν_μ flux, which can be tied to the ν_e flux, and through the measurement of ν_e CCQE events.

Once the muon neutrino flux is measured to high precision, it can be used to constrain the electron neutrino flux. This is because the ν_e ($\bar{\nu}_e$) background is largely due to K^+ (K^-) decays in neutrino (antineutrino mode). Using the measured ν_μ peak from K^+ events, the beam Monte Carlo can be precisely tuned. Having measured the CCQE cross section precisely in the process of determining the ν_μ flux, this result can then be applied to ν_e CCQE events to cross check the ν_e flux prediction.

4   Preliminary Design

This report focuses upon the determination of the physics goals of the experiment. In order to maintain realistic goals, we have developed a preliminary design for a beam and detector based on existing technology. There are two particularly challenging aspects of the design. The first is the high Tevatron intensity discussed in sec. 4.1. The second is the high precision required for the detector calibration discussed in sec. 4.3.3.

The 2007 Fermilab Steering Group Report considers the Tevatron-based neutrino beam described here. The preliminary concept for the facility recieved an endorsement [137].

4.1   Proton Delivery to NuSOnG

Our goal is to obtain 2×10^{20} protons on target during a 5-year run. This section outlines how we might achieve this goal.

Proton delivery occurs via the following lines:

- The Linac
- The Booster
- The Main Injector
- The Tevatron
- Extraction to targeting

The existing Linac and the Booster should perform to the level needed by NuSOnG without problems. The Booster fills the MI in batches of 5×10^{12} protons and will operate between 9 and 15 Hz by 2015. The Proton Plan projects 7×10^{13} protons in each MI fill by 2010 [138]. Two pulses from the MI are used to fill the Tevatron. In principle, therefore, it is conceivable that the Tevatron could receive nearly 1.5×10^{14} protons per fill under this scenario.

Let's suppose that with care the Tevatron can accelerate 8×10^{13} ppp to 800 GeV using two pulses from the Main Injector at 4×10^{13} each pulse, similar to today's MI operation. To date, the highest intensities extracted from the Tevatron in a single pulse at 800 GeV were around 2.5 to 3×10^{13}. The limiting issue was longitudinal instabilities for energies above 600 GeV at high intensities, as the bunch length shrank. "Bunch spreaders" were used to compensate. A better method to compensate will be required for NuSOnG. However, advances in rf techniques and technology and in damper systems make finding a satisfactory solution conceivable. More detailed study is needed.

Our proposal is for a Tevatron cycle time of 40 s, with a 1 s flattop at 800 GeV. Since the MI cycle time will be 2.2 s, and we need two injections, our impact on NuMI is $4.4/40 = 11\%$ of their run time.

If the uptime for the Tevatron is 66%, then we will receive 5×10^5 cycles per year. At 8×10^{13} ppp, this gives 4×10^{19} protons per year. We then achieve our goal in five years of running.

4.2   Neutrino Beam Design

4.2.1   Target

Beryllium oxide was the target material in NuTeV and prior high energy neutrino beamlines [140, 141]. Beryllium is efficient at producing secondary mesons, and BeO has good structural and thermal properties. The NuTeV target consisted of two 30 cm long, 2.5 cm diameter segmented rods in a copper cooling block, mounted on a movable drive that could select between centering the beam on either of the two targets or no target. This target was designed to accept up to 1×10^{13} protons per pulse (ppp). A similar target will be acceptable for NuSOnG, but it may be a challenge to provide adequate cooling at our design intensity of 8×10^{13} protons per cycle. The NuTeV protons were delivered in five 4 msec "pings" separated by 0.5 sec; we intend to have one pulse of about 200 msec. This means that our instantaneous heating rate will be somewhat lower than NuTeV's, but the total number of protons per cycle is eight times higher. In NuTeV the beam width was 0.6 mm, which was significantly smaller than necessary; a wider more diffuse beam would help relieve the localized heating problem. Careful design of the target support and cooling system will be a necessity.

4.2.2   SSQT

A Sign Selecting Quadrupole Train (SSQT) can be used to provide beams of either neutrinos or antineutrinos with very low contamination from either wrong-sign muon neutrinos or electron neutrinos from neutral kaons. The NuTeV SSQT utilized two dipoles and six quadrupoles, with two dumps [140, 141]. The first dipole provided a 6.1 mrad bend for 250 GeV daughter mesons of the selected sign. In antineutrino mode the unreacted protons are bent in the opposite direction and are absorbed in the first dump. In neutrino mode the protons are absorbed in the second dump. The first two quadrupoles capture the secondary beam. A second dipole then bends the beam by another 1.6 mrad, enhancing the sign separation and sweeping out low energy particles produced by scraping in upstream magnets. Neutral particles are not bent and therefore travel away from the detector. NuSOnG will use a similar SSQT. The only challenge will be designing the proton dumps for our significantly higher intensity. In the NuTeV upstream dump in antineutrino mode, the dump temperature approached 100 C at 1.3×10^{13} protons per pulse; the temperature limit was 110 C. The NuSOnG dumps will need to be water-cooled.

4.2.3   Monitoring

Primary beam monitoring in NuTeV was accomplished with four beam position monitors (BPMs), four vacuum segmented wire ionization chambers (SWICs), four secondary emission electron detectors (SEEDs), a beam current toroid, and a thin foil secondary emission monitor (SEM) [140, 141]. The toroid, SEM, SEEDs and BPMs measured proton intensity; the BPMs, SWICs, and SEEDs monitored position. It was found that the SEM degraded over the course of the run, so the beam toroid was used as the primary measure of intensity. The BPMs and SEEDs gave closely correllated position measurements, and the SWICs and SEEDs gave beam profiles that agreed well except in the tails; the SEED tails dropped more rapidly than those from the SWICs. With the exception of the SEMs, which would suffer even more radiation damage at

Parameter	Value
Total target mass	3.492
Fiducial mass	2.975 kt
Total length	192 m
Number of glass planes	2500
Number of toroid washers	96
Number of muon detector wire planes (two coordinates each)	60

Table 3: Summary of NuSOnG detector parameters.

our higher intensities, a combination of any of these monitoring devices could be used by NuSOnG.

4.3 Detector Design

This section details our first ideas about the detector configuration; these are summarized in Tab. 3. In thinking about NuSOnG, we have drawn on previous large, high energy neutrino detectors whose characteristics are summarized in Table 4. NuSOnG represents a natural evolution of these designs and we believe this makes construction low risk. Of particular note regarding Table 4 is the excellent performance achieved by CHARM II using digital proportional tubes, a glass target, and fine granularity.

The primary event signatures NuSOnG will need to identify are:

- charged current deep inelastic scattering, characterized by a hadronic shower and a high energy muon

- neutral current deep inelastic scattering, characterized by a hadronic shower

- inverse muon decay, $\nu_\mu + e^- \rightarrow \mu^- + \overline{\nu}_e$, which is characterized by a high energy muon accompanied by no hadronic activity.

- neutrino and antineutrino electron scattering, characterized by an electromagnetic shower with no hadronic activity

- stopped muon decay, which results in an electromagnetic shower with energy up to 50 MeV. These events will be used to reject low hadronic energy events which are tagged through the $\pi \rightarrow \mu \rightarrow e$ decay chain (see sec. 3.3.1).

In order to achieve the rates and carry out the measurements given in Section 3, NuSOnG consists of a 3.5 kton (3 kton fiducial volume) isoscalar target with high segmentation resulting in good separation between electromagnetic and hadronic showers and muon tracks with good energy resolution for each. Good separation between hadronic and electromagnetic showers and good muon identification are necessary for separation of neutral and charged current events, and for low systematic errors on the measurements of the neutrino and antineutrino electron scattering cross sections. Finally, good muon identification is critical for detecting inverse muon decay events for a precise flux measurement.

Given the large size of the detector, ease of construction and low cost technologies are important. The long running time requires high stability and robust operation.

	Resolution			Sampling	Absorber
	EM (σ_E/E)	Hadronic (σ_E/E)	Muon (σ_p/p)		
FMMF (Flash tubes, digital)	$1.04/\sqrt{E}$	$0.72/\sqrt{E}$	8%	0.11 X_o	sand/shot
CDHS (Scintillator)	$0.80/\sqrt{E}$	-	5%	2.8/8.3 X_o	steel
CHARM II (Prop. tubes, digital)	$0.52/\sqrt{E}+0.02$	$0.24/\sqrt{E}+0.34$	5%	0.5 X_o	glass
NuTeV (Scintillator)	$0.86/\sqrt{E}+0.022$	$0.5/\sqrt{E}+0.042$	10%	5.8 X_o	steel

Table 4: Comparison of high energy neutrino detectors.

Our first design is shown in Figs. 14 and 15 and summarized in Table 3. NuSOnG consists of four calorimeters each with a muon spectrometer. 15 m decay volumes separate the four detector elements. Interspersing the decay volumes between the detectors will allow a calibration beam to be brought to each of the four detector regions.

Each calorimeter has 500 SiO_2 2.5 cm ($X_o/4$) glass target planes interleaved with active detectors with two dimensional readout. The active detectors could be proportional tubes, scintillator panels, or a combination of both. These three options are discussed below. Neutrinos interact in the target planes, creating secondary particles; the active detector determines the total energies of the hadronic and electromagnetic secondaries. The muon detector measures the momentum of muon secondaries and serves to identify them. The pattern of the shower serves to identify the shower type: showers in which all the energy resides in ten of fifteen planes will be electromagnetic, and more extended showers will be hadronic. The lateral extent of the shower also resolves electromagnetic from hadronic showers.

We have chosen an SiO_2 target. This material provides a balance between longer radiation length, important to particle ID issues, and shorter detector length, important for acceptance and calibration issues. The target could be commercial glass or thin walled plastic boxes filled with sand. Glass planes have the advantage of being easy to install and require no construction. Sand-filled boxes could be much less expensive. We will investigate both possibilities. Either way, SiO_2 has the advantage of being isoscalar ($\langle N_u \rangle > /\langle N_d \rangle$=0.998). SiO_2 has a density of 2.2 g/cm^3; a high energy muon will lose 10 MeV per plane, which gives 5 GeV across all 500 planes in one calorimeter. Energy loss will also occur through electromagnetic showers. An example straight-through muon event from our initial GEANT4 detector simulation is shown in Fig. 16. A michel electron with 30 MeV energy should be clearly visible across three planes. Each calorimeter is followed by a toroidal muon spectrometer consisting of magnetized iron plates interleaved with drift chambers.

Other target materials, including emulsion, are under consideration, as has been discussed in previous sections of this document. These materials are not yet incor-
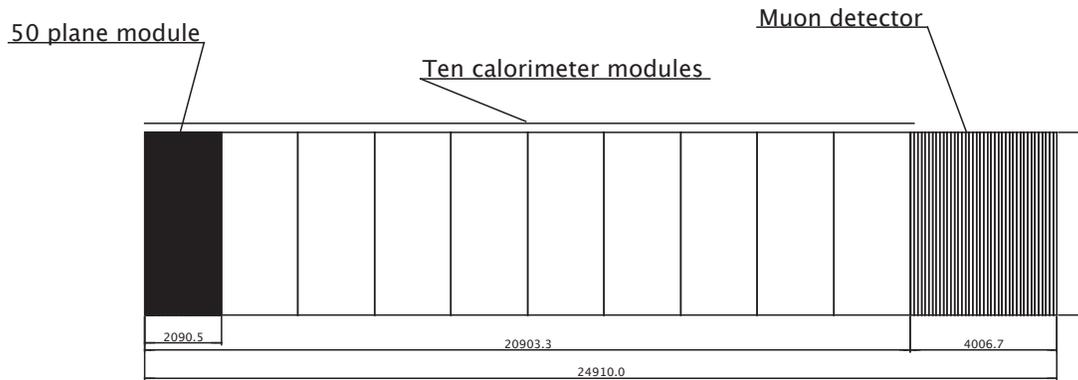
50 plane module

Ten calorimeter modules

Muon detector

2090.5

20903.3

4006.7

24910.0

Figure 14: NuSOnG detector showing calorimeter modules and muon detector.
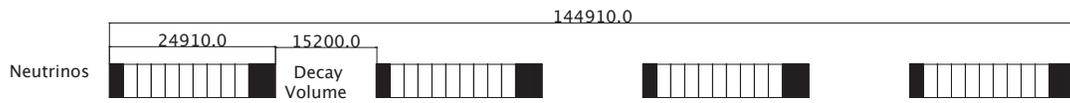

144910.0

24910.0

15200.0

Neutrinos

Decay
Volume

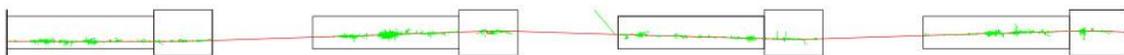Figure 15: The full NuSOnG experiment showing four detectors separated by a decay volume.

Figure 16: A 100 GeV muon traversing the detector from the NuSOnG initial GEANT4 Monte Carlo.

porated into the preliminary design presented here, but should be straightforward to include in the future.

The design must address beam correlated backgrounds. These include backgrounds arising from debris (muons, remnants of hadronic showers) from neutrino interactions in the earth surrounding the detector. We plan for a forward veto consisting of a three layer scintillator hodoscope. Since our detector is so long, we may also need a veto system along the sides, top, and bottom of the calorimeters. We plan a Monte Carlo study of veto requirements in the coming months. Cosmic rays muons and their attendant showers present a beam-uncorrelated background which we will need to eliminate. We envisage a counter on the top of the detector similar to that used by the MINOS experiment.

NuTeV showed the value of continuous beam calibration and this will be discussed in a separate section.

While our detector is quite large, the robust, simple design will make the cost and construction manageable. The modules design makes upgrades and improvements straightforward. While we are designing with an initial four to five year run in mind, this detector can be put to other uses should the physics warrant.

4.3.1 Active detector options

The active detector performs two roles: first, it tracks the particles emerging from a neutrino interaction; second, it samples the particle's energy loss along the trajectory giving an measurement of the total energy. Simplicity, robustness, and high efficiency are essential, as is low cost.

Two technologies immediately present themselves: gas-filled proportional tubes and plastic scintillator read out by phototubes. Both have been used in several experiments (see Table 4). At this point, it is not clear to us which is the best approach for NuSOnG. We are also considering a design with both proportional tubes and scintillator. In the coming months, we plan to study the performance of each via simulation, develop preliminary design prototypes, and carry out a detailed cost estimate. We describe each detector concept below.

4.3.1.1 Proportional Tubes

A first design for a proportional tube active detector is shown in Fig. 17. Each active detector plane is made from five 1 m × 5 m extruded aluminum panels. Each panel contains fifty 1 cm × 2 cm drift cells. A 50 μm wire is strung down the center of each tube, and the applied high voltage produces both drift and proportional amplification fields. Ar:CO_2 (80:20) provides a good candidate for a fill gas; with 1.8 - 2 kV applied to the wire, the drift field will give a drift velocity of about 50 μm/ns and a gain of 3000. A minimum ionizing particle crossing the 1 cm cell will deposit 2.7 keV of energy, liberating about 160 drift electrons in ten or so clusters. The drift time across the cell will be about 500 ns and proportional multiplication will give a collected charge of 80 fC over a time of 250 ns.

As an example of a readout scheme, we look to the ATLAS Transition Radiation Tracker (TRT) ASIC chips. The TRT readout has a peaking time of 7.5 ns and a charge threshold of 2 fC, making them well matched to our proportional tubes. Each chip set reads out sixteen channels and can be configured to provide trigger information.
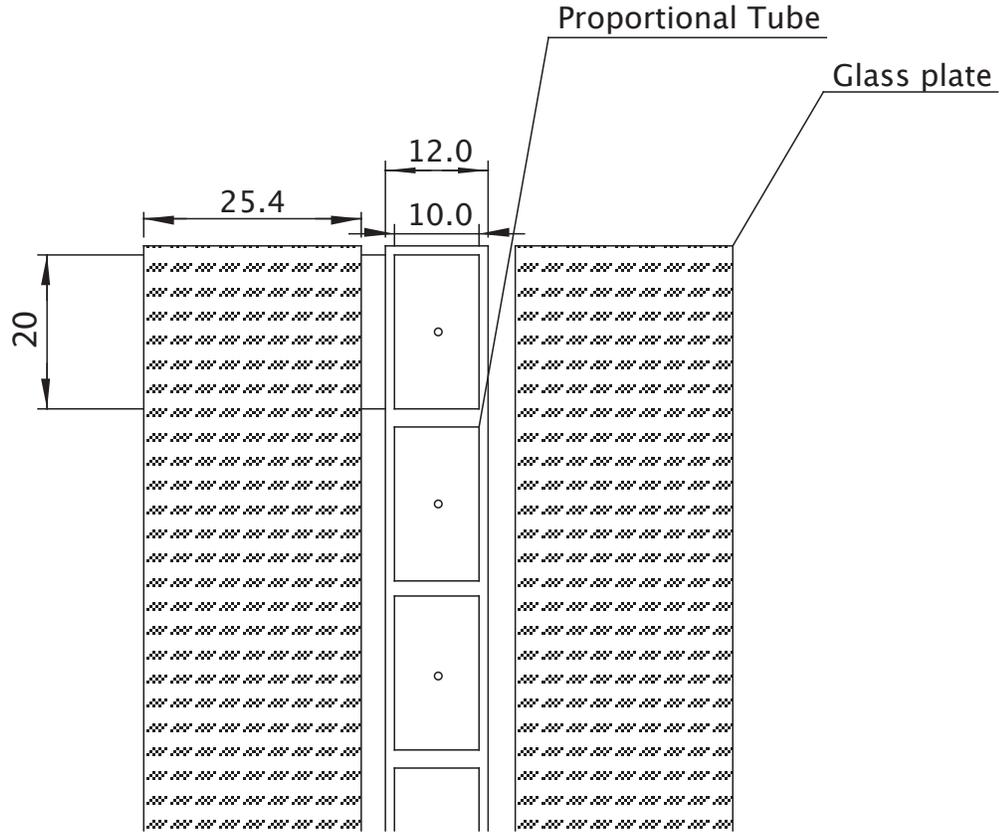
51

Figure 17: Proportional tubes design.

The TRT system, which is based around 6 mm straw tubes, has achieved a spatial resolution of 127 μm, albeit with higher energy deposition resulting from the use of a xenon mixture. Scaling by the energy deposition gives a resolution of 200μm for our argon-filled tubes. The TRT readout chip set has sufficient charge sensitivity to allow us to use charge division; this should give position resolution of 5-10 cm along the wire.

4.3.1.2 Scintillating Strips

The second option uses planes of scintillator strips read out with green wavelength-shifting fibers fed into multi-anode photomultipliers. This option would be similar to that used for the SciBar detector in K2K, the Minos neutrino detector, and the Opera neutrino detector. NuSOnG would have 2500 5 m by 5 m planes with each plane made up of 128 3.9 cm × 1.3 cm strips. Each 64 strip plane will be separately wrapped in an Al skin that will provide the light seal and strength for the module.

The scintillator strips will be coextruded with a TiO_2 reflective coating and have a 1.8 mm diameter hole in the middle. A 1.5 mm diameter green wavelength-shifting fiber will be put in the hole and routed to multianode photomultipliers for readout. The 64

wavelength-shifting fibers on one side of a plane will be coupled to a Hamamatsu M64 multianode photomultiplier tube. The readout side will alternate between subsequent planes to improve uniformity. The fiber end opposite to the tubes will be polished and mirrored to increase the light output and uniformity. Planes will alternate between horizontal and vertical strips to provide two view tracking; readout tubes will alternate.

The readout would be based on a custom ASIC combined with a standard FPGA. One example is the 64 channel MAROC2 custom integrated circuit, designed at LAL (Orsay) for the ATLAS luminosity monitor. This chip allows adjustment of the electronic gain of each of the 64 channels, which will be needed to correct for the expected factor of 3 pixel-to-pixel gain variation of the M64 tubes. The system provides a self-triggering analog readout into an external flash ADC. A fast discriminator signal for triggering is also available for each strip with a common threshold.

Based on the performance of the SciBar detector, a minimum ionizing particle traversing a strip will yields about 20 photoelectons close to the tube, and the strip/fiber system will have an attenuation length of 3.5 m. This would then produce about 10 photoelectrons at the center of the detector per plane.

4.3.1.3   Hybrid Design

Our initial estimates indicate the scintillator option may cost more than the proportional tube option. However, the scintillator system described above does provide a stable, easy to characterize active detector. In particular, scintillating strips offer very stable response that does not vary with pressure or temperature. We will investigate a hybrid system in which every fourth or eighth plane (one or two radiation lengths) would be a scintillator panel. The high granularity of the proportional tube design would give good pattern recognition, and the excellent energy resolution of the scintillator would give a better energy measurement. Reducing the fiber spacing in the scintillator may be possible; this would reduce the cost.

One issue with adding 12-25% scintillator would be the change in the fraction of protons in the detector. The precise change depends on the scintillator used, but for CH_4 and one scintillator panel every quarter radiation length, the proton-neutron ratio changes from 0.998 to 0.940. The impact of this change will have to be balanced against the cost reduction and stability improvement. This will be part of our Monte Carlo effort in the coming months.

4.3.2   Toroid Spectrometers

High energy muons produced in charged-current interactions will be momentum analyzed in three iron toroid spectrometers downstream of each subdetector (set of ten "stacks"). Each spectrometer will be composed of layers of magnetized iron instrumented with drift chambers for tracking.

Since NuSOnG will see muons of the same energies as NuTeV/CCFR a similar arrangement for measuring muon momenta would be suitable. CCFR used sections of 8" thick steel washers instrumented with scintillator hodoscopes for calorimeter.[2]

---

[2]The CCFR arrangement used two C-shaped sections with a horizontal crack at the center to allow placement of hall probes for field calibration. This crack would be eliminated in NuSOnG and instead small slots could be included for this purpose.
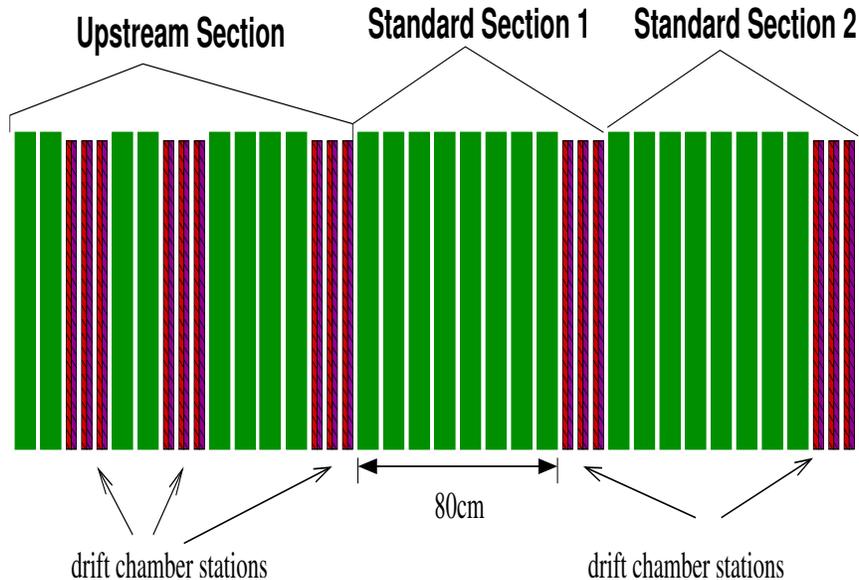
Figure 18: Conceptual Schematic for a NuSOnG toroid element. The three sections contain the same amount of steel (eight washers of 8" each). The upstream most section has additional drift chamber stations to improve acceptance for low energy muons. Each of the five drift chamber stations has 3x and 3y view chambers.

Tracking was performed using four views of each x and y chambers (0.5 mm coordinate resolution) in three gaps located after each 1.6 m of steel. The magnetic field was produced by four coils carrying approximately 1500 A each which passed through the center hole. The field was nearly radially symmetric and pointed in the azimuthal direction with magnitude ranging from 1.9 T near the center hole to 1.55 T near the outer edge (at R=1.8 m). Details can be found in reference [142].

Figure 18 shows a possible arrangement for a NuSOnG toroid spectrometer. One "Upstream section" and two downstream "Standard sections" are shown. The downstream sections contain eight 8" washers with one drift chamber station with 3x and 3y view chambers each. The most upstream section of a spectrometer unit has two additional drift chamber stations to improve acceptance for low energy muons. To pass the coil through this arrangement the upstream chamber stations would be half size (the same chambers but rotated for each view). Each of the three sections contain the same amount of steel. Hodoscope paddles could be added in each chamber station for triggering purposes. Resolution of this arrangement would be dominated by multiple Coulomb scattering and would be $\sim 11\%$ independent of momentum.

The NuSOnG arrangement will provide good acceptance for high energy primary muons of both signs since in a sign-selected beam the can be routinely operated with the polarity set to focus the primary muon. Very high energy particles can be tracked into the downstream target sections with a long lever arm and their momentum analyzed. (resolution for very high energy muons ($> 150 \text{GeV}$ was limited in NuTeV and CCFR; this resulted in large uncertainties in measuring flux in the high energy tail of the beam). Improving flux measurements in this region may help constrain kaon fluxes and therefore electron neutrino beam contamination.

4.3.3 Detector Calibration

A thorough and precise calibration of the entire detector will be required to achieve the physics goals of NuSOnG. Some of the response features of the detector can be understood using beam and cosmic ray muon samples, but a dedicated calibration effort will be required to study the hadronic and electromagnetic response of the detector and to measure the absolute energy scales. Precise calibration of a detector of this size will require a dedicated *in situ* calibration beam such as was used in NuTeV for this purpose [143].

The requirements for NuSOnG calibration beam would be similar to those of NuTeV. Tagged beams of hadrons, electrons, and muons over a wide energy range (5-200 GeV) would be required. The calibration beam should have the ability to be steered over the transverse face of the detector in order to map the magnetic field of each toroid with muons. This could be accomplished in several ways; for example, gaps of a few meters in front of each toroid could be incorporated into the design, and the beam could be steered into each toroid in turn; or the toroids could each be moved into the test beam for these calibration runs. Steering for hadrons and electrons would be less crucial than it was in NuTeV's case but would still be useful.

The calibration beam can be constructed with a similar design to NuTeV. Upstream elements were used to select hadrons, electrons, or muons. An enhanced beam of electrons was produced by introducing a thin lead radiator into the beam and detuning the portion of the beam downstream of the radiator. A radiator was also used in the nominal beam tune to remove electrons. Particle ID (a threshold cerenkov and TRDs) was incorporated in the spectrometer and used to tag electrons when running at low energy. A pure muon beam was produced by introducing a 7 m long beryllium filter in the beam as an absorber.

The NuTeV calibration spectrometer was able to determine incoming particle momenta with a precision of better than 0.3% absolute. This was accomplished by two means. First, precisely calibrated dipole spectrometer magnets were used, with $\int B d\ell$ known to better than 0.1% in the region traversed by the beam. Secondly, the bend angle was determined to better than 0.1% using drift chambers positioned over the 150 m spectrometer. This long lever arm allowed a modest alignment uncertainty of a few mm to translate into only a 0.1% uncertainty in the absolute momentum scale. The event-by-event resolution of the spectrometer, dominated by multiple scattering in the drift chamber walls, was better than 0.3% for most energies. (Helium in the region between the last dipole and the upstream part of the detector reduced the scattering in air).

Figure 19 shows the NuTeV calibration beam configuration and the long lever arm spectrometer used to tag particle momenta with an absolute precision of better than 0.3%. The most downstream dipole was mounted on a rotating stand which gave the ability to steer the beam out of the plane.

The NuSOnG goal of the calibration precision would be to measure energy scales to a precision of about 0.5%. NuTeV achieved 0.43% precision on absolute hadronic energy scale and 0.7% on absolute muon energy scale (dominated by the ability to accurately determine the toroid map). Precise knowledge of the muon energy scale is especially important in order to achieve high measurement accuracy on the neutrino fluxes using the low-ν method. For example a 0.5% precision on muon energy scale translates into about a 1% precision on the flux. Both energy scales are important
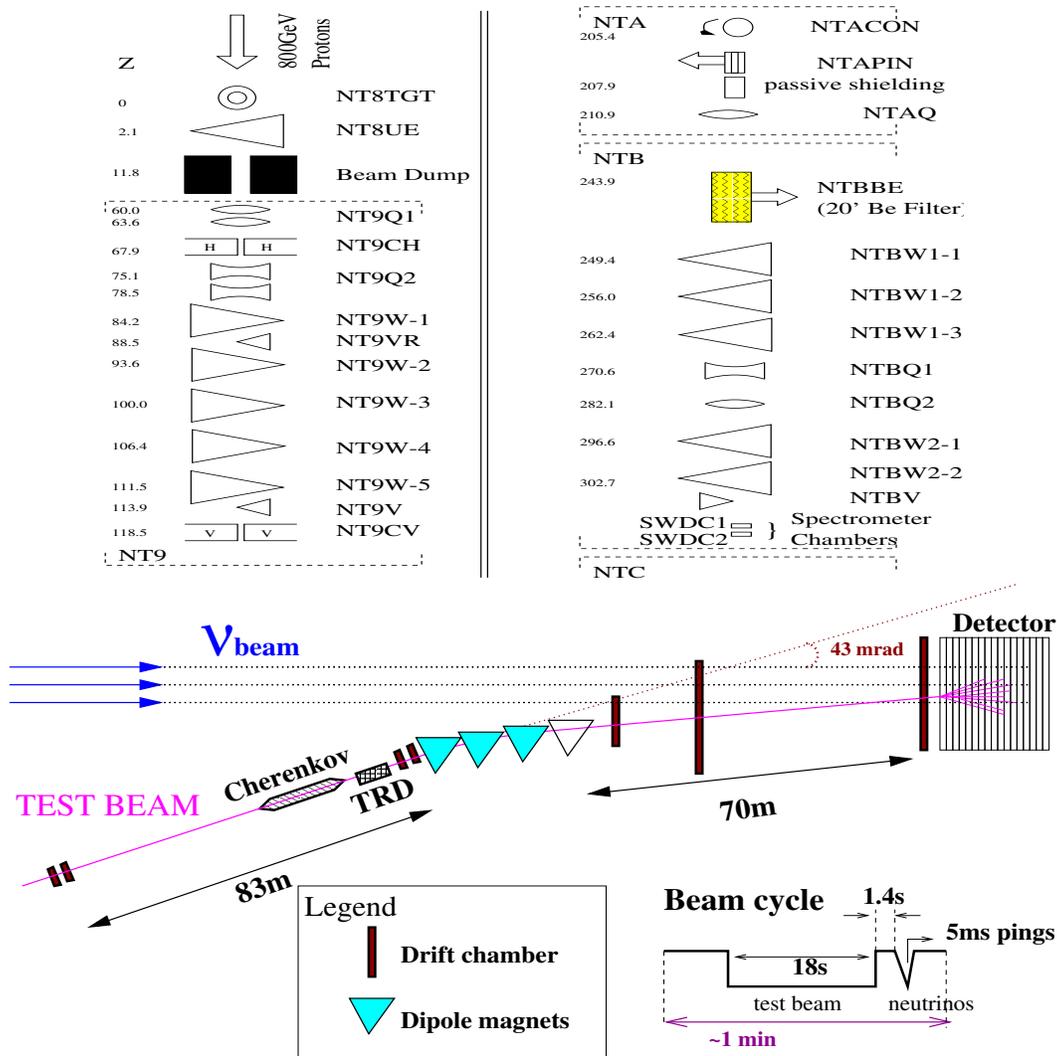
Figure 19: (Top) Components of the NTEST beamline used to calibrate the NuTeV detector. Four different thicknesses of converter material at NTACON were used to select pure hadrons or electrons. The 7 m long Be filter(NTBBE) was used to select pure muons. The numbers on the left-hand-side of each component indicate the relative distance of the component to the primary target (NT8TGT) in meters. (Bottom) NuTeV's long lever arm spectrometer. The four dipole bend magnets were located in an enclosure approximately 70 m upstream of the Lab E detector. The spectrometer spanned over 150 m in length; this allowed precision measurement of the bending angle.

for precision structure function measurements and were the largest contributions to structure function measurement uncertainties in NuTeV [89].

4.4   Possible Locations

Fig. 20 shows a possible location for the NuSOnG beam target hall and detector. Other layouts are possible; this is just meant to provide an example.

This layout assumes that the beam is extracted at A0 from the TeVatron and directed through the Switchyard Complex to a new targeting hall. This location allows low luminosity extraction down existing beamlines for the calibration beam.

The detector is located near the New Muon Lab. This is a region with more than 200 m of clear length, with roads and utilities nearby.

The calibration beam could be delivered to the NuSOnG hall using a scheme similar to that used in NuTeV with the NTest beamline. Only a short extension of the existing NTest line would be required to reach a detector located near the New Muon Lab. The beam was split off from the same beamline (Ncenter) and then bent around to impinge on the detector at a 43 mrad angle.
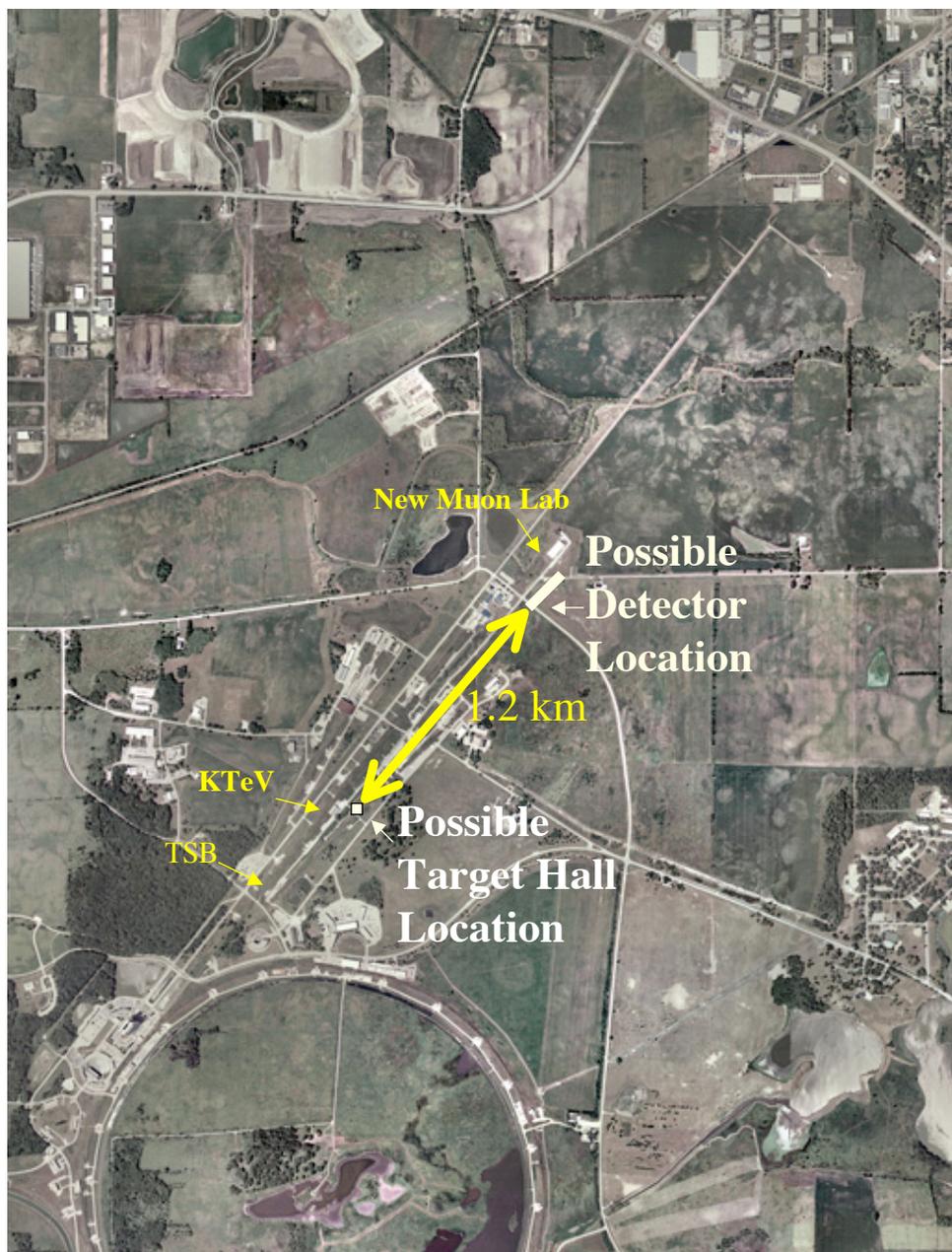
Figure 20: Aerial view of Fermilab showing the Tevatron, external beam lines and potential site for NuSOnG target and detector halls.

5 Summary

NuSOnG is an experimental program with high discovery potential. The precision neutrino scattering measurements probe terascale physics and will complement discoveries at the LHC. Through precision electroweak measurements, NuSOnG will be sensitive to such new phenomena as extra Z bosons with masses beyond the 1 TeV (depending on the model) and compositeness scales above 5 TeV. The NuSOnG measurement of the coupling to the Z, when combined with the LEP measurement of the invisible width, is a more sensitive method to search for new physics than this same measurement at the ILC. NuSOnG can also probe the existence of neutrissimos, moderately heavy neutral heavy leptons which may be produced at the LHC, but which could be difficult to reconstruct and identify. A wide range of direct searches for new particles and interactions can be accomplished. The high neutrino flux and isoscalar target will make allow measurements which probe deeper into nuclear structure.

The high energy neutrino facility, which uses 800 GeV protons from the TeVatron, has been endorsed by the 2007 Fermilab Steering Group. While NuSOnG is the first to propose an experiment for this facility, a wide range of interesting measurements can be made on this line.

The proposed 3 kton (fiducial) NuSOnG detector design, which is opitmized for the physics goals, is based largely on the experiences of NuTeV and CHARM II. The basic technology is straightforward, although challenges exist because of the high precision demanded by the physics goals. Detailed simulations of the detector are now underway

Our plan is to develop these ideas over the coming months. We plan to submit a proposal to the Fermilab Directorate in the near future.

References

[1] P. Vilain *et al.*, Phys. Lett. B335: 246, 1994.

[2] J. Erler and P. Langacker, "Electroweak Model and Constraints on New Physics," http://pdge.lbl.gov/2006/reviews/stanmodelrpp.pdf

[3] E. A. Paschos and L. Wolfenstein, Phys. Rev. D **7**, 91 (1973).

[4] G. P. Zeller *et al.* Phys. Rev. Lett., **88** 091802, 2002.

[5] M. Carena, A. de Gouvea, A. Freitas, and M. Schmitt, Phys. Rev. D **68**, 113007 (2003) [arXiv:hep-ph/0308053].

[6] ElectroWeak Working Group, ALEPH, DELPI, L3, OPAL, and SLD Collaborations, arXiv:hep-ex/0212036.

[7] M. E. Peskin and T. Takeuchi, Phys. Rev. D **46**, 381 (1992).

[8] J. L. Rosner, Phys. Rev. D **70**, 037301 (2004) arXiv:hep-ph/0404264.

[9] http://lepewwg.web.cern.ch/LEPEWWG/

[10] M. E. Peskin and J. D. Wells, Phys. Rev. D **64**, 093003 (2001) [arXiv:hep-ph/0101342].

[11] T. Takeuchi and W. Loinaz, arXiv:hep-ph/0410201.

[12] W. Loinaz, N. Okamura, S. Rayyan, T. Takeuchi, and L. C. R. Wijewardhana, Phys. Rev. D **68**, 073001 (2003) [arXiv:hep-ph/0304004].

[13] A. de Gouvea, arXiv:0706.1732 [hep-ph].

[14] E. Prebys, *et al.*, http://www.fnal.gov/directorate/Longrange/Steering_Public/files/EOI_mu2e.pdf.

[15] N. Sahu and U. A. Yajnik, Phys. Rev. D **71**, 023507 (2005) [arXiv:hep-ph/0410075].

[16] A. de Gouvea, J. Jenkins, and N. Vasudevan, Phys. Rev. D **75**, 013003 (2007) [arXiv:hep-ph/0608147].

[17] B. W. Lee, C. Quigg, and H. B. Thacker, Phys. Rev. D **16**, 1519 (1977).

[18]

[19] G. D. Kribs, T. Plehn, M. Spannowsky, and T. M. P. Tait, arXiv:0706.3718 [hep-ph].

[20] A. Ceccucci, Z. Legeti, and Y Sakai, http://pdg.lbl.gov/2007/reviews/kmmixrpp.pdf

[21] . B. A. Dobrescu and C. T. Hill, Phys.Rev.Lett.81:2634-2637,1998; R.S. Chivukula, B. A. Dobrescu, H. Georgi, and C. T. Hill, Phys.Rev.D59:075003,1999.

[22] C.T. Hill, private communication.

[23] P. Langacker and M. x. Luo, Phys. Rev. D **45**, 278 (1992); G. Altarelli, R. Casalbuoni, S. De Curtis, N. Di Bartolomeo, R. Gatto, and F. Feruglio, Phys. Lett. B **318**, 139 (1993). T. G. Rizzo, Phys. Rev. D **50**, 2256 (1994) [arXiv:hep-ph/9403241].

[24] J. Erler and P. Langacker, arXiv:hep-ph/0407097.

[25] M. Carena, A. Delgado, E. Ponton, T. M. P. Tait, and C. E. M. Wagner, Phys. Rev. D **68**, 035010 (2003) [arXiv:hep-ph/0305188].

[26] J. L. Hewett, F. J. Petriello, and T. G. Rizzo, JHEP **0310**, 062 (2003) [arXiv:hep-ph/0211218].

[27] C. T. Hill and E. H. Simmons, Phys. Rept. **381**, 235 (2003) [Erratum-ibid. **390**, 553 (2004)] [arXiv:hep-ph/0203079].

[28] O. C. Anoka, K. S. Babu, and I. Gogoladze, Nucl. Phys. B **687**, 3 (2004) [arXiv:hep-ph/0401133]; M. Cvetic and P. Langacker, arXiv:hep-ph/9707451.

[29] M. Carena, E. Ponton, T. M. P. Tait, and C. E. M. Wagner, Phys. Rev. D **67**, 096006 (2003) [arXiv:hep-ph/0212307].

[30] A. Birkedal, K. T. Matchev, and M. Perelstein, *In the Proceedings of 2005 International Linear Collider Workshop (LCWS 2005), Stanford, California, 18-22 Mar 2005, pp 0314* [arXiv:hep-ph/0508185].

[31] http://www.slac.stanford.edu/exp/e158/

[32] G.P. Zeller, private communication.

[33] G. P. Zeller, "A precise measurement of the weak mixing angle in neutrino nucleon scattering," (Thesis) UMI-30-50615

[34] S. C. Bennett and Carl E. Wieman, Phys. Rev. Lett., **82** 2484–2487, 1999.

[35] P. L. Anthony *et al.* [SLAC E158 Collaboration], Phys. Rev. Lett. **95**, 081601 (2005) [arXiv:hep-ex/0504049].

[36] K. P. O. Diener, S. Dittmaier, and W. Hollik, Phys. Rev. D **69**, 073005 (2004) [arXiv:hep-ph/0310364].

[37] K. S. McFarland and S. O. Moch, arXiv:hep-ph/0306052.

[38] S. Davidson, S. Forte, P. Gambino, N. Rius, and A. Strumia, JHEP **0202**, 037 (2002) [arXiv:hep-ph/0112302].

[39] K. S. McFarland and S. O. Moch, arXiv:hep-ph/0306052; S. Kretzer and M. H. Reno, Phys. Rev. D **69**, 034002 (2004) [arXiv:hep-ph/0307023]; B. A. Dobrescu and R. K. Ellis, Phys. Rev. D **69**, 114014 (2004) [arXiv:hep-ph/0310154].

[40] M. Gluck, P. Jimenez-Delgado, and E. Reya, arXiv:hep-ph/0501169; F. M. Steffens and K. Tsushima, Phys. Rev. D **70**, 094040 (2004) [arXiv:hep-ph/0408018]; J. T. Londergan and A. W. Thomas, arXiv:hep-ph/0407247; A. D. Martin, R. G. Roberts, W. J. Stirling, and R. S. Thorne, Eur. Phys. J. C **39**, 155 (2005) [arXiv:hep-ph/0411040].

[41] G. P. Zeller *et al.* [NuTeV Collaboration], Phys. Rev. D **65**, 111103 (2002) [Erratum-ibid. D **67**, 119902 (2003)] [arXiv:hep-ex/0203004].

[42] F. Olness *et al.*, Eur. Phys. J. C **40**, 145 (2005) [arXiv:hep-ph/0312323].

[43] V. Barone, C. Pascaud, and F. Zomer, Eur. Phys. J. C **12**, 243 (2000) [arXiv:hep-ph/9907512].

[44] R.N. Mohapatra *et al.*, hep-ph/050213v2, 2005.

[45] S. Davidson, J. Phys. G **29**, 2001 (2003) [arXiv:hep-ph/0209316].

[46] E. Ma, D. P. Roy, and S. Roy, Phys. Lett. B **525**, 101 (2002) [arXiv:hep-ph/0110146].

[47] B. T. Cleveland *et al.*, Astrophys. J. **496**, 505 (1998).

[48] Y. Fukuda *et al.* [Super-Kamiokande Collaboration], Phys. Rev. Lett. **81**, 1158 (1998) [Erratum-ibid. **81**, 4279 (1998)] [arXiv:hep-ex/9805021]; Phys. Rev. Lett. **82**, 2430 (1999) [arXiv:hep-ex/9812011].

[49] J. N. Abdurashitov *et al.* [SAGE Collaboration], J. Exp. Theor. Phys. **95**, 181 (2002) [Zh. Eksp. Teor. Fiz. **122**, 211 (2002)] [arXiv:astro-ph/0204245].

[50] W. Hampel *et al.* [GALLEX Collaboration], Phys. Lett. B **447**, 127 (1999).

[51] M. Altmann *et al.* [GNO Collaboration], Phys. Lett. B **490**, 16 (2000) [arXiv:hep-ex/0006034].

[52] Q. R. Ahmad *et al.* [SNO Collaboration], Phys. Rev. Lett. **89**, 011301 (2002) [arXiv:nucl-ex/0204008]; Phys. Rev. Lett. **89**, 011302 (2002) [arXiv:nucl-ex/0204009]; Phys. Rev. Lett. **87**, 071301 (2001) [arXiv:nucl-ex/0106015].

[53] T. Araki *et al.* [KamLAND Collaboration], Phys. Rev. Lett. **94**, 081801 (2005) [arXiv:hep-ex/0406035].

[54] Y. Fukuda *et al.* [Super-Kamiokande Collaboration], Phys. Lett. B **433**, 9 (1998) [arXiv:hep-ex/9803006]; Phys. Lett. B **436**, 33 (1998) [arXiv:hep-ex/9805006]; Phys. Rev. Lett. **81**, 1562 (1998) [arXiv:hep-ex/9807003]; Phys. Rev. Lett. **82**, 2644 (1999) [arXiv:hep-ex/9812014]; Phys. Lett. B **467**, 185 (1999) [arXiv:hep-ex/9908049]; Y. Ashie *et al.* [Super-Kamiokande Collaboration], Phys. Rev. D **71**, 112005 (2005) [arXiv:hep-ex/0501064].

[55] D. Casper *et al.*, Phys. Rev. Lett. **66**, 2561 (1991); R. Becker-Szendy *et al.*, Phys. Rev. Lett. **69**, 1010 (1992).

[56] M. Ambrosio *et al.* [MACRO Collaboration], Phys. Lett. B **434**, 451 (1998) [arXiv:hep-ex/9807005]; Phys. Lett. B **478**, 5 (2000) [arXiv:hep-ex/0001044]; Phys. Lett. B **517**, 59 (2001) [arXiv:hep-ex/0106049]; Phys. Lett. B **566**, 35 (2003) [arXiv:hep-ex/0304037].

[57] W. W. M. Allison *et al.*, Phys. Lett. B **391**, 491 (1997) [arXiv:hep-ex/9611007]; Phys. Lett. B **449**, 137 (1999) [arXiv:hep-ex/9901024]; M. C. Sanchez *et al.* [Soudan 2 Collaboration], [arXiv:hep-ex/0307069].

[58] S. H. Ahn *et al.* [K2K Collaboration], Phys. Lett. B **511**, 178 (2001) [arXiv:hep-ex/0103001]; Phys. Rev. Lett. **90**, 041801 (2003) [arXiv:hep-ex/0212007]; Phys. Rev. D **74**, 072003 (2006) [arXiv:hep-ex/0606032].

[59] D. G. Michael *et al.* [MINOS Collaboration], [arXiv:hep-ex/0607088].

[60] M. Apollonio *et al.*, Eur. Phys. J. C **27**, 331 (2003) [arXiv:hep-ex/0301017].

[61] T. Araki *et al.* [KamLAND Collaboration], [arXiv:hep-ex/0406035].

[62] A. A. Aguilar-Arevalo *et al.* [The MiniBooNE Collaboration], arXiv:0704.1500 [hep-ex].

[63] M. Maltoni and T. Schwetz, [arXiv:hep-ph/0705.0107].

[64] Boris Kayser, private communication.

[65] S. Antusch *et al.*, [arXiv:hep-ph/0607020].

[66] K. Abazajian, G. M. Fuller, and M. Patel, [arXiv:astro-ph/0101524].

[67] I.E. Stockdale *et al.*, Phys. Rev. Lett. **52**, 1384 (1984); Z. Phys. C **27**, 53 (1985).

[68] F. Dydak *et al.*, Phys. Lett. B **134** 281, 1984.

[69] P. Astier *et al.* Phys. Lett. B570:19, 2003; hep-ex/0306037.

[70] G. Ambrosini *et al.* [NA56/SPY Collaboration], Eur. Phys. J. C **10**, 605 (1999); G. Ambrosini *et al.* [SPY Collaboration], Phys. Lett. B **425**, 208 (1998).

[71] G. Feinberg and S. Weinberg, Phys. Rev. Lett. **6**, 381 (1961)

[72] A. Ibarra, E. Masso, and J. Redondo, Nucl. Phys. B **715**, 523 (2005) [arXiv:hep-ph/0410386].

[73] P. Herczeg and R. N. Mohapatra, Phys. Rev. Lett. **69**, 2475 (1992).

[74] S. Godfrey, P. Kalyniak, and N. Romanenko, Phys. Rev. D **65**, 033009 (2002) [arXiv:hep-ph/0108258].

[75] J. A. Formaggio *et al.* [NuTeV Collaboration], Phys. Rev. Lett. **87**, 071803 (2001) [arXiv:hep-ex/0104029].

[76] W. Fetscher, H. J. Gerber, and K. F. Johnson, *In *Heidelberg 1986, Proceedings, Weak and electromagnetic interactions in nuclei* 812-815. (see Conference Index)*

[77] Roesch, L.Ph. et al., Helv. Phys. Acta 55 (1982) 74. Abela, R. et al., Nucl. Phys. Lett. A39(1984) 413.

[78] W. M. Yao *et al.* [Particle Data Group], J. Phys. G **33**, 1 (2006).

[79] T. Adams *et al.* [NuTeV Collaboration], Phys. Rev. Lett. **87**, 041801 (2001) [arXiv:hep-ex/0104037].

[80] V. M. Abazov *et al.* [D0 Collaboration], Phys. Rev. Lett. **97**, 161802 (2006) [arXiv:hep-ex/0607028].

[81] A. Dedes, H. K. Dreiner, and P. Richardson, Phys. Rev. D **65**, 015001 (2002) [arXiv:hep-ph/0106199].

[82] L. Okun, Phys. Lett. B **382**, 389 (1996) [arXiv:hep-ph/9512436].

[83] P. Vilain *et al.* [CHARM II Collaboration], Phys. Lett. B **434**, 200 (1998).

[84] S. Kretzer, H. L. Lai, F. I. Olness, and W. K. Tung, Phys. Rev. D **69**, 114005 (2004) [arXiv:hep-ph/0307022].

[85] . CCFR Collaboration: W. G. Seligman *et al.*, Phys. Rev. Lett. **79**, 1213 (1997) [hep-ex/970107]; CCFR Collaboration: U. K. Yang *et al.*, Phys. Rev. Lett. **86**, 2742 (2001) [hep-ex/0009041].

[86] . U. K. Yang *et al.* [CCFR/NuTeV Collaboration], arXiv:hep-ex/9806023.

[87] M. Arneodo *et al.* [New Muon Collaboration], Nucl. Phys. B **483**, 3 (1997) [arXiv:hep-ph/9610231].

[88] J. M. Conrad, M. H. Shaevitz, and T. Bolton, Rev. Mod. Phys. **70**, 1341 (1998) [arXiv:hep-ex/9707015].

[89] M. Tzanov *et al.*, Phys. Rev. D **74**, 012008 (2006).

[90] G. Onengut *et al.*, Phys. Lett. B **632**, 65 (2006).

[91] J.F. Owens *et al.*, Phys. Rev. D **75**, 054030 (2007) [hep-ph/0702159].

[92] S.A. Kulagin and R. Petti, Nucl. Phys. A **765**, 126 (2006)

[93] C. Boros, F. M. Steffens, J. T. Londergan, and A. W. Thomas, Phys. Lett. B **468**, 161 (1999) [arXiv:hep-ph/9908280].

[94] R. D. Ball, D. A. Harris, and K. S. McFarland, arXiv:hep-ph/0009223.

[95] S. Kretzer, F. I. Olness, R. J. Scalise, R. S. Thorne, and U. K. Yang, Phys. Rev. D **64**, 033003 (2001) [arXiv:hep-ph/0101088].

[96] A. D. Martin, R. G. Roberts, W. J. Stirling, and R. S. Thorne, Eur. Phys. J. C **23**, 73 (2002) [arXiv:hep-ph/0110215].

[97] F. Abe *et al.* [CDF Collaboration], Phys. Rev. Lett. **81**, 5754 (1998) [arXiv:hep-ex/9809001].

[98] A. Bodek, Q. Fan, M. Lancaster, K. S. McFarland, and U. K. Yang, Phys. Rev. Lett. **83**, 2892 (1999) [arXiv:hep-ex/9904022].

[99] A. Baldit *et al.* [NA51 Collaboration], Phys. Lett. B **332**, 244 (1994).

[100] E. A. Hawker *et al.* [FNAL E866/NuSea Collaboration], Phys. Rev. Lett. **80**, 3715 (1998) [arXiv:hep-ex/9803011].

[101] K. S. McFarland *et al.*, arXiv:hep-ex/0205080.

[102] A. Strumia, arXiv:hep-ex/0304039.

[103] A. O. Bazarko *et al.* [CCFR Collaboration], Z. Phys. C **65**, 189 (1995) [arXiv:hep-ex/9406007].

[104] M. Goncharov *et al.* [NuTeV Collaboration], Phys. Rev. D **64**, 112006 (2001) [arXiv:hep-ex/0102049].

[105] M. Tzanov *et al.* [NuTeV Collaboration], arXiv:hep-ex/0306035.

[106] P. Vilain *et al.* [CHARM II Collaboration], Eur. Phys. J. C **11**, 19 (1999).

[107] P. Astier *et al.* [NOMAD Collaboration], Phys. Lett. B **486**, 35 (2000).

[108] D. A. Mason, "Measurement of the strange - antistrange asymmetry at NLO in QCD from NuTeV dimuon data," (Thesis) UMI-32-11223. A paper is in draft.

[109] M. Nakamura, private communication.

[110] B. Fleming *et al.*, http://www.fnal.gov/directorate/Longrange/Steering_Public/files/Neutrino_Fleming.pdf

[111] P. H. Sandler *et al.*, Phys. Rev. D **42**, 759 (1990).

[112] P. H. Sandler *et al.*, Z. Phys. C **57**, 1 (1993).

[113] P. H. Sandler, "Neutrino production of same sign dimuons at the Fermilab tevatron," (Thesis) UMI-92-18364-MC.

[114] W.G. Seligman, Ph. D. Thesis, Nevis Report 292.

[115] P.S. Auchincloss *et al.*, Z. Phys. **C48**, 411 (1990).

[116] D.B. MacFarlane *et al.*, Z. Phys. **C26**, 1 (1984).

[117] P. Berge *et al.*, Z. Phys. **C35**, 443 (1987).

[118] J. Morfin *et al.*, Phys. Lett. **104B**, 235 (1981).

[119] D.C. Colley *et al.*, Z. Phys. **C2**, 187 (1979).

[120] S. Campolillo *et al.*, Phys. Lett. **84B**, 281 (1979).

[121] O. Erriquez *et al.*, Phys. Lett. **80B**, 309 (1979).

[122] V.B. Anikeev *et al.*, Z. Phys. **C70**, 39 (1996).

[123] A.S. Vovenko *et al.*, Sov. J. Nucl. Phys. **30**, 527 (1979).

[124] D.S. Baranov *et al.*, Phys. Lett. **81B**, 255 (1979).

[125] C. Baltay *et al.*, Phys. Rev. Lett. **44**, 916 (1980).

[126] S.J. Barish *et al.*, Phys. Rev. **D19**, 2521 (1979).

[127] N.J. Baker *et al.*, Phys. Rev. **D25**, 617 (1982).

[128] J.V. Allaby *et al.*, Z. Phys. **C38**, 403 (1988).

[129] W. Seligman and M. Shaevitz, private communication.

[130] D. Casper, Nucl. Phys. Proc. Suppl. **112**, 161 (2002) [arXiv:hep-ph/0208030].

[131] D. Naples, talk given at NuINT07.

[132] P. Vilain *et al.* [CHARM-II Collaboration], Phys. Lett. B **364**, 121 (1995).

[133] A. A. Aguilar-Arevalo *et al.* [MiniBooNE Collaboration], arXiv:0706.0926 [hep-ex].

[134] A. A. Aguilar-Arevalo *et al.* [SciBooNE Collaboration], arXiv:hep-ex/0601022.

[135] J. G. Morfin and K. McFarland, "Proposal to perform a high - statisics neutrino scattering experiment using a fine - grained detector in the NuMI Beam," FERMILAB-PROPOSAL-0938.

[136] A. Bodek, S. Avvakumov, R. Bradford, and H. Budd, arXiv:0708.1946 [hep-ex].

[137] The Fermilab Steering Group Report can be found at: http://www.fnal.gov/directorate/Longrange/Steering_Public/

[138] The Fermilab Proton Plan is available from E. Prebys, head of the Booster Dept., prebys@fnal.gov.

[139] S. E. Kopp, Phys. Rept. **439**, 101 (2007) [arXiv:physics/0609129].

[140] R. Bernstein et al.; "Sign-Selected Quadrupole Train"; FERMILAB-TM-1884, April 1994

[141] J. Yu et al.; "NuTeV SSQT Performance"; FERMILAB-TM-2040,February 1998

[142] B. J. King *et al.*, Nucl. Inst. Meth. **A302**, 254, 1991.

[143] D. A. Harris *et al.*, Nucl. Instrum. Methods **A447** (2000) 377.